Geological Society of America
Special Paper 374
2003

# *Late Cretaceous cooling of the east-central Peninsular Ranges batholith (33°N): Relationship to La Posta pluton emplacement, Laramide shallow subduction, and forearc sedimentation*

**Marty Grove**
**Oscar Lovera**
*Department of Earth and Space Sciences, University of California, 595 Charles Young Drive E, Los Angeles, California 90095-1567, USA*

**Mark Harrison**
*Department of Earth and Space Sciences, University of California, 595 Charles Young Drive E, Los Angeles, California 90095-1567, USA, and Research School of Earth Sciences, The Australian National University, Canberra, ACT 0200, Australia*

## ABSTRACT

**Biotite and K-feldspar $^{40}Ar/^{39}Ar$ systems from the east-central Peninsular Ranges batholith near 33°N were affected by two distinct phases of Late Cretaceous rapid cooling. The 85-Ma biotite K-Ar isochron separates comparatively shallow rocks in the southwest that record earlier cooling (91–86 Ma) from deeper rocks in the northeast that record later cooling (78–68 Ma). Samples close to 85 Ma isochron record both episodes of rapid cooling as well as slower cooling between 86 and 78 Ma. Although the 85 Ma isochron also coincides with a steep (1–2 m.y./km) K-Ar age gradient, only localized faulting has been detected along it. We attribute 91–86 Ma cooling to denudation related to emplacement of the voluminous suite of 96 ± 3 Ma La Posta plutons. In contrast, we link cooling after 78 Ma to Laramide shallow subduction beneath the Peninsular Ranges batholith. Our numerical simulations indicate that the latter cooling phase can be explained by either pure erosional denudation or by subduction refrigeration beginning at 80 Ma. In the latter case, erosional denudation occurs during steady-state shallow subduction. While final erosion depths predicted by the two models differ significantly (as much as 20 km for pure erosional denudation but only 11 km for subduction refrigeration followed by erosion), both are within the range indicated by independent thermobarometry of the eastern batholith. Based upon the similarity of independently determined denudation histories from Peninsular Ranges batholith basement rocks and forearc sediments that onlap the northern Peninsular Ranges batholith, we conclude that erosional denudation was probably the most important process between 78 and 68 Ma. We speculate that removal of lower crust and lithospheric mantle beneath the east-central Peninsular Ranges batholith during Laramide shallow subduction triggered erosional denudation and localized thrusting until the density balance between the crust and mantle was restored in latest Cretaceous–early Tertiary time.**

**Keywords:** Peninsular Ranges, denudation, Laramide, La Posta plutons, thermochronology.

*Marty@oro.ess.ucla.edu

Grove, M., Lovera, O., and Harrison, M., 2003, Late Cretaceous cooling of the east-central Peninsular Ranges batholith (33°N): Relationship to La Posta pluton emplacement, Laramide shallow subduction, and forearc sedimentation, *in* Johnson, S.E., Paterson, S.R., Fletcher, J.M., Girty, G.H., Kimbrough, D.L., and Martín-Barajas, A., eds., Tectonic evolution of northwestern México and the southwestern USA: Boulder, Colorado, Geological Society of America Special Paper 374, p. 355–379. 

## INTRODUCTION

A fundamental and incompletely understood aspect of crustal evolution is the response of continental arcs to the thermal and gravitational anomalies generated by batholith emplacement. The first-order expectation is that exhumation, erosion, faulting, and related processes should be most active during and immediately following intrusion when temperatures are high and rocks are weak (e.g., Tobisch et al., 1995). As thermal and density differences decay, the crust should strengthen and resist further mechanical readjustment unless triggered by changes in tectonic regime (e.g., Chase and Wallace, 1986).

Episodes of enormous magmatic influx are a hallmark of the medial Cretaceous Cordilleran magmatic arcs distributed along western North America (e.g., Bateman and Chappell, 1979; Barton et al., 1988; Coleman and Glazner, 1998; Ducea, 2001). The best examples of this phenomena are the distinctive large-volume, Late Cretaceous tonalite-trondhjemite-granodiorite (TTG) plutons that dominate the eastern Peninsular Ranges batholith of southern and Baja California (Gastil et al., 1975; Gastil, 1983; Taylor, 1986; Gromet and Silver, 1987; Todd et al., 1988; Silver and Chappell, 1988; Hill, 1988; Clinkenbeard and Walawender, 1989; Walawender et al., 1990; Gastil et al., 1991; Fig. 1). Walawender et al. (1990) coined the term "La Posta–type plutons" for these intrusions, and we follow Kimbrough et al. (1998) in referring to them as the La Posta TTG suite. The La Posta TTG suite is the defining characteristic of the Peninsular Ranges batholith. It occurs as a series of large, internally zoned intrusive centers that are distributed throughout the entire 800 km length of the batholith (Fig. 1; Gastil et al., 1975; Kimbrough et al., 2001). Available geologic mapping, geochronology, and geophysical data indicate that the suite represents a magmatic influx of ~75–100 $km^3$/km of batholith strike length/m.y. from ca. 98 to 93 Ma and that roughly 50% of the total exposed area of the batholith was emplaced during this surprisingly brief interval (Silver and Chappell, 1988; Kimbrough et al., 1998; Kimbrough et al., 2001).

It is reasonable to expect that injection of such an enormous quantity of magma into the crust over a short period would have had a profound impact upon the evolution of the Peninsular Ranges batholith. At its more shallowly denuded southern end, this appears to have been the case. Extensive exhumation and forearc sedimentation directly overlapped intrusion of the La Posta TTG and little has happened since (Kimbrough et al., 2001). In the more heavily denuded northern Peninsular Ranges batholith, however, the correspondence between La Posta TTG intrusion and exhumation is less clear. The ambiguity stems from the fact that large tracts of the La Posta TTG–dominated eastern batholith apparently required 15–20 Ma from the time of their emplacement to cool below the ~350 °C temperature (McDougall and Harrison, 1999) required for Ar diffusion in biotite (Armstrong and Suppe, 1973; Krummenacher et al., 1975; Goodwin and Renne, 1991; George and Dokka, 1994; Grove, 1994; Naeser et al., 1996; Ortega-Rivera et al., 1997; Ortega-Rivera, 2003). In fact, it has been proposed that significant post-batholithic, Late Cretaceous cooling of the northern Peninsular Ranges batholith occurred primarily in two discrete phases: 1) closely following emplacement of the La Posta TTG during the Cenomanian–Turonian, and (2) 15–20 m.y. later during the Late Campanian–Maastrictian (Grove, 1994; Lovera et al., 1999).

The Late Campanian–Maastrictian timing of the second phase of cooling suggests a causal relationship with Laramide shallow subduction (ca. 80–45 Ma; e.g., Coney and Reynolds, 1977; Dickinson and Snyder, 1978; Bird, 1988). The probability that Laramide shallow subduction occurred beneath the Peninsular Ranges is indicated by the Late Cretaceous migration of the magmatic arc into the formerly adjacent regions of Sonora (e.g., Gastil and Krummenacher, 1977; Silver et al., 1996; Staude and Barton, 2001; McDowell et al., 2001; Ortega-Rivera, 2003). Grove et al. (2003b) and Barth et al. (2003) have demonstrated that the Rand Schist and schists of Sierra de Salinas and Portal Ridge were underplated beneath the southern Sierra Nevada batholith and equivalent arc rocks of Salinia (southern Coast Ranges) and the western Mojave region between ca. 90 and 75 Ma. Projecting this relationship to the south, Grove et al. (2003b) speculated that schist of equivalent age was also accreted beneath the Peninsular Ranges batholith. Hence, subduction-induced cooling (i.e., subduction refrigeration) of the overriding crust may have occurred beneath the Peninsular Ranges in the same manner as has been proposed for the Sierra Nevada batholith (Dumitru, l990; Dumitru et al., 1991).

Subduction refrigeration is not the only expected consequence of Laramide shallow subduction. The most widely accepted model for the underplating of the Pelona and related schists involves tectonic removal of the mantle lithosphere and basal crust (Burchfiel and Davis, 1981; Crowell, 1981; Hamilton, 1988; Bird, 1988). There is evidence that a similar process could have occurred beneath the eastern Peninsular Ranges batholith. During emplacement of the La Posta TTG, the thickness of the crust in the eastern batholith is likely to have been well in excess of 40 km (Gromet and Silver, 1987). Present-day crustal thickness within the eastern Peninsular Ranges batholith is considerably thinner (~30 km) with no Airy root evident (Lewis et al., 2001). Removal of the crustal root during Laramide shallow subduction would have destabilized the overlying crust and triggered denudation to restore the density balance between the crust and the upper mantle.

In this study, we have performed detailed thermochronology based upon $^{40}Ar/^{39}Ar$ analysis of K-feldspar (Lovera et al., 1989, 1993, 1997, 2002) and other phases to better understand the timing and magnitude of cooling in an area (east-central Peninsular Ranges batholith at 33°N) that is dominated by the immense (>1500 $km^2$) La Posta pluton sensu stricto (e.g., Miller, 1935) and related TTG intrusives (Fig. 2). Our analysis clearly documents the two phases of rapid cooling described above. We further conclude that Cretaceous, east-side up, semi-ductile to brittle fault zones may locally have played an important role in producing the sharp age gradients observed across the 85 Ma biotite K-Ar isochron. Using our thermal history results, we numerically evaluate

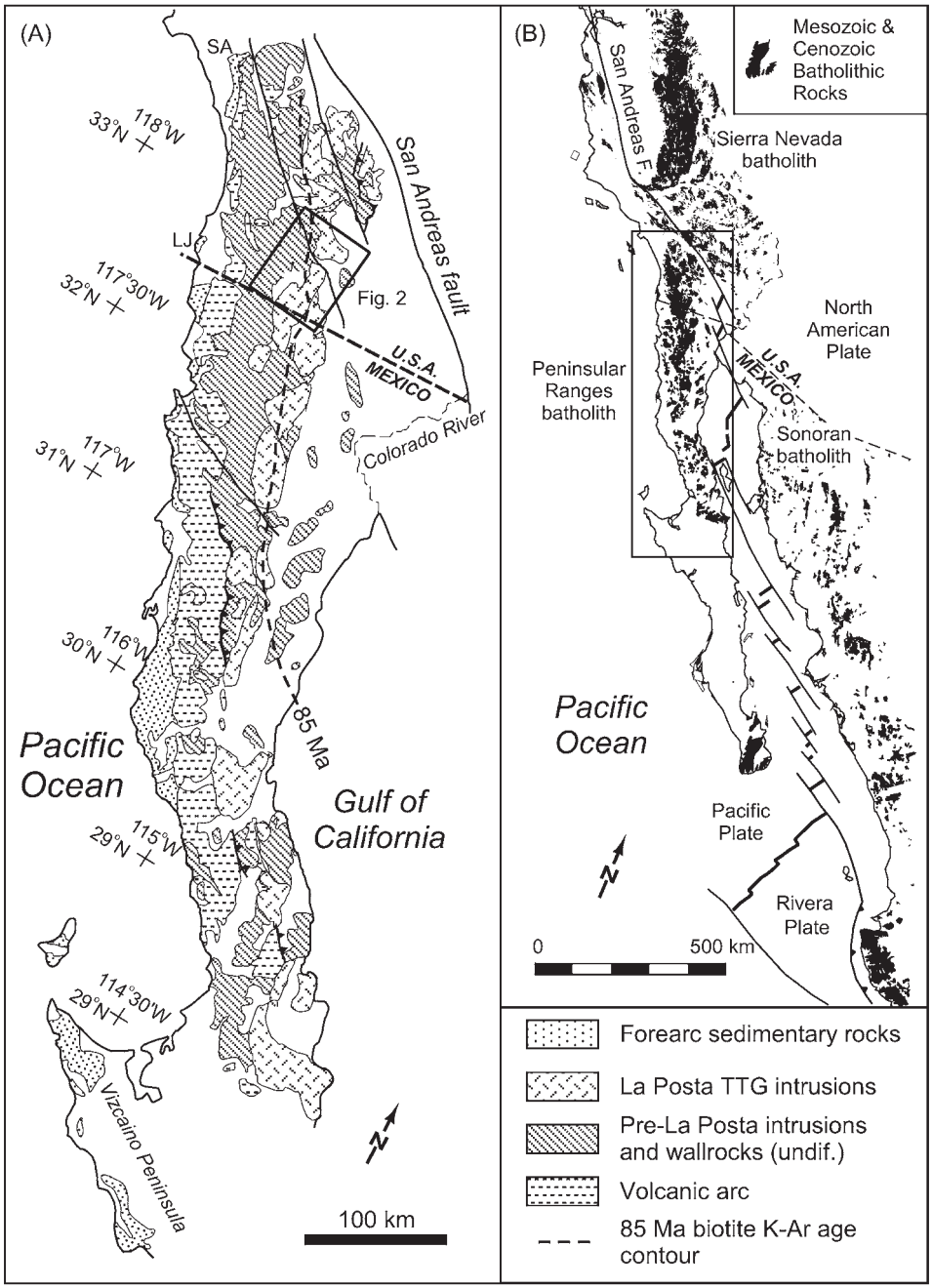


Figure 1. A: Geologic sketch map of Peninsular Ranges batholith. Distribution of La Posta tonalite-trondjemhite-granodiorite (TTG) suite is after Kimbrough et al. (2001). Location of the 85 Ma biotite K-Ar age isochron based upon Krummenacher et al. (1975), Ortega-Rivera (2003), and this study. Location of Figure 2 (east-central batholith at 33°N) is indicated by the open box. SA—Santa Ana Mountains and LJ—La Jolla are localities from the Peninsular Ranges batholith forearc that are discussed in text. B: Geologic setting of Peninsular Ranges batholith. Distribution of Mesozoic and Cenozoic granitic rocks of southwestern North America adapted from Jennings (1977) and Ortega-Gutierrez et al. (1992). Northern Peninsular Ranges batholith (outlined by rectangular area) was adjacent to Sonoran batholith of mainland México prior to late Tertiary opening of Gulf of California and development of San Andreas transform system.

crustal scale models for the Late Cretaceous (erosion denudation and Laramide subduction refrigeration). We conclude that while both processes can account for important aspects of our thermal history results, independent data from the forearc favors erosional denudation as the controlling mechanism.

## BACKGROUND

The Peninsular Ranges batholith is characterized by numerous strike parallel, lithologic, and compositional belts and has traditionally been subdivided into western and eastern zones on the basis of pluton composition, size, style of emplacement, age, and isotopic considerations (Fig. 2; Gastil et al., 1975; DePaolo, 1981; Baird and Miesch, 1984; Taylor, 1986; Hill et al., 1986; Jachens et al., 1986; Gromet and Silver, 1987; Silver and Chappell, 1988; Todd et al., 1988; Ague and Brimhall, 1988; Gastil et al., 1990, 1991; Walawender et al., 1990).

Prebatholithic host rocks of the studied area are predominately early Mesozoic(?) "sandstone-shale" slope margin lithologies (Gastil, 1993) that are referred to locally as Julian Schist

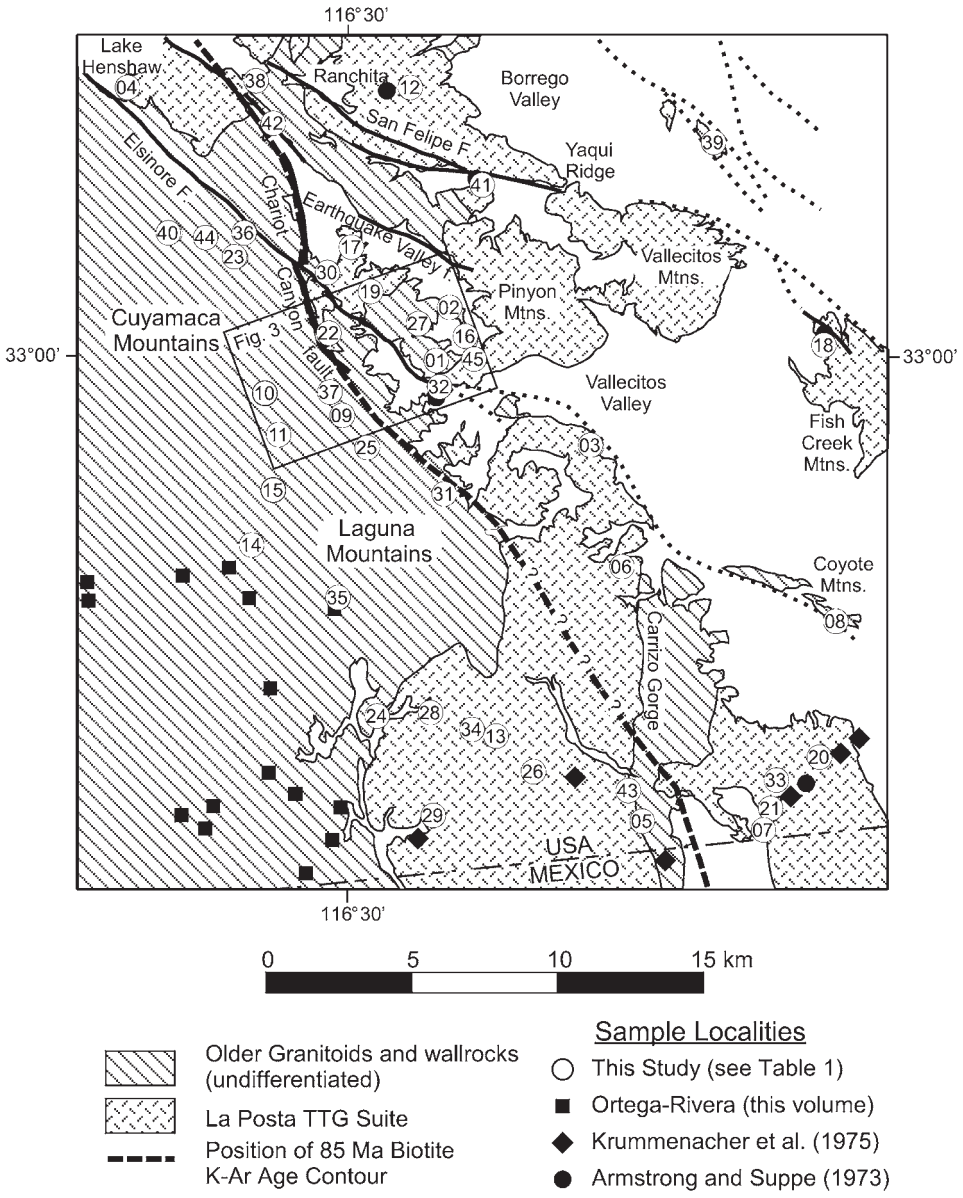


Figure 2. Geologic sketch map of study area in east-central Peninsular Ranges batholith near 33°N. Distribution of La Posta tonalite-trondhjemite-granodiorite (TTG) intrusions from Strand (1962), Todd (1977a, 1978, 1979), Todd and Shaw (1979), Todd et al. (1988), personal communication with Dave Kimbrough, and field observations. Position of 85-Ma biotite isochron is same as in Figure 1. Numbers within circles correspond to sample localities in Table 1. Lake Henshaw–Ranchita, Chariot Canyon–Granite Mountain, Carrizo Gorge, Yaqui Ridge, and Coyote Mountains are localities discussed in text. Location of Figure 3 is outlined by rectangle.

(Fig. 3). Quartz and carbonate-rich wallrocks with miogeoclinal affinities and radiogenic $^{87}Sr/^{86}Sr$ (0.706–0.708) in plutons from the northeastern part of Figure 2 (Yaqui Ridge, Coyote Mountains) suggest that this portion of the study area is probably underlain by cratonal basement (DePaolo, 1981; Silver and Chappel, 1988; Gastil, 1993).

Most intrusions in the western portion of Figure 2 are ca. 125–100 Ma "I-type" quartz monzonite, granodiorite, tonalite, and gabbro bodies with generally primitive isotopic signatures (Everhart, 1951; Merriam, 1958; DePaolo, 1981; Todd and Shaw, 1985; Taylor, 1986; Silver and Chappell, 1988; Todd and Shaw, 2003). Also abundant are Middle Jurassic, compositionally heterogeneous and strongly deformed "S-type" granitoids (referred to as Cuyamaca granodiorite and Harper Creek gneiss in Fig. 3) that are intimately intermingled with Julian Schist over broad regions (Everhart, 1951; Merriam, 1958; Todd and Shaw, 1985; Todd et al., 1988; Thomson and Girty, 1994; Shaw et al., 2003). While Cretaceous western zone plutons are generally only weakly deformed throughout the western batholith, they are locally strongly attenuated within the Cuyamaca–Laguna Mountains shear zone (Fig. 3; Todd and Shaw, 1979; Todd et al., 1988; Thomson and Girty, 1994; Todd et al., 2003).

Intrusion of the La Posta TTG suite postdated shearing along the Cuyamaca–Laguna Mountains shear zone (Todd et al., 2003). The rocks underlie much of the eastern portion of Figure 2. Generally massive to strongly foliated, hornblende-biotite ± clinopyroxene tonalite of Granite Mountain is intruded by the massive and generally undeformed La Posta pluton (Todd,

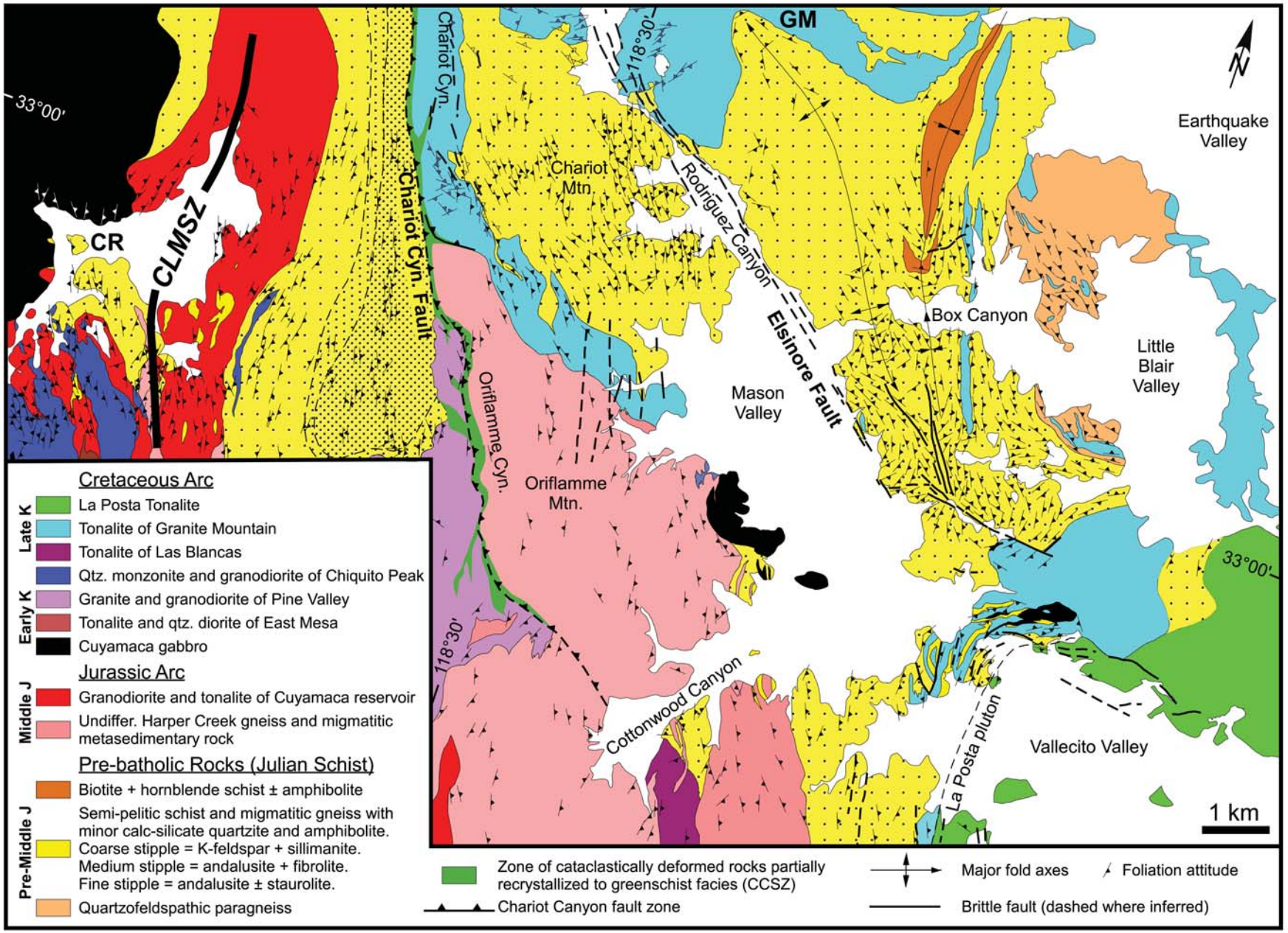


Figure 3. Geologic map of Cuyamaca Reservoir (CR)–Granite Mountain (GM) region. Map relations from Phillips (1964), Todd (1977a, 1977b, 1978, 1979), Grove (1987), Lampe (1988), Germinario (1994), and Grove (1994). Cuyamaca–Laguna mountain shear zone (CLMSZ) and Chariot Canyon fault zone are discussed in text.

1977a, Todd et al., 1988; see Fig. 3). Ubiquitous, fine- grained biotite granodiorite and swarms of subparallel tabular garnetiferous, two-mica pegmatites are broadly coeval with the La Posta suite rocks (Gastil et al., 1991). Locally, tight- to isoclinal, shallow-plunging, north- to northwest-trending folds deform both the tonalite of Granite Mountain and the granite pegmatites that crosscut it (Fig. 3; Phillips, 1964; Grove, 1987). Foliation surfaces expressed in both intrusive units are transposed parallel to the intrusive contact with the essentially undeformed and areally extensive La Posta pluton.

### Basement Cooling Age Patterns and Relationships to Intrusion and Forearc Sedimentation

Post–93 Ma cooling within the east-central Peninsular Ranges batholith near 33°N occurred after volumetrically significant intrusion had ceased within the region (Silver et al., 1988; Todd et al., 1988). Late Cretaceous plutonism (to ca. 65 Ma; Anderson and Silver, 1974; Gastil and Krummenacher, 1977; Silver and Chappell, 1988) took place within formerly adjacent rocks (e.g., Silver et al., 1996) across the Gulf of California in mainland Sonora, México (Fig. 1). However, the thermal effects related to these bodies would have reached only a few kilometers at most (e.g., Hanson and Barton, 1989). West of the Salton Trough, a few zircon U/Pb and mineral Rb/Sr isochron ages determined for pegmatites and muscovite granites are younger than 93 Ma (e.g., Parrish, 1990). Because they are volumetrically minor, these late-stage intrusions are unlikely to have induced significant $^{40}$Ar loss from K-Ar thermochronometers through the eastern Peninsular Ranges batholith. Moreover, although larger granitoids yielding U-Pb zircon ages as young as 75 Ma do crop out within the Sierra Cucapá (Silver and Chappell, 1988; Grove et al., 2003a) and other ranges within the Salton Trough (Premo et al., 1998), biotite and K-feldspar $^{40}$Ar/$^{39}$Ar ages obtained from them are generally 10–20 Ma younger than the time of intrustion (Axen et al., 2000; M. Grove, unpubl. data). Hence, even in these areas, there is no compelling case for $^{40}$Ar loss due to transient heating effects associated with pluton emplacement. Consequently, we consider that biotite and K-feldspar Ar isotopic ages from the eastern Peninsular Ranges batholith at 33°N represent regional cooling patterns in a deep crustal setting (see also Krummenacher et al., 1975).

Krummenacher et al.'s (1975; see also Ortega-Rivera, 2003) 85 Ma biotite K-Ar isochron provides a convenient way of delineating rocks with contrasting cooling histories within the east-central Peninsular Ranges batholith near 33°N. Krummenacher et al. (1975) demonstrated that the positions of the 90 Ma and older biotite K-Ar isochrons were strongly influenced by the boundaries of plutons of the La Posta TTG suite while younger contours (including 85 Ma) are superposed across these intrusions (Fig. 1). Both Silver et al. (1979) and Grove (1994) have described a sharp eastward decrease in K-Ar cooling ages that occurs across the 85-Ma biotite K-Ar isochron. We will use the position of the 85 Ma contour as a geographic reference line throughout this paper.

West of the 85-Ma biotite K-Ar isochron, biotite records early Late Cretaceous (Turonain–Cenomanian) cooling in comparatively shallow rocks (2–3 kbar or 7–11 km; see Berggreen and Wallawender, 1977; Detterman, 1984; Todd et al., 1988; Germinario, 1993; Grove, 1994; Rothstein and Manning, this volume, Chapter 12). Development of poorly dated (Cenomanian–Turonian?), west-flowing, steep gradient, short-length streams and numerous alluvial fan/submarine fan masses (Flynn, 1970; Nordstrom, 1970; Kennedy and Moore, 1971; Peterson and Nordstrom, 1970; Sundberg and Cooper, 1978; Bottjer and Link, 1984) appear to record contemporaneous erosional denudation. Results of Lovera et al. (1999) from the Peninsular Ranges batholith forearc confirm that significant erosional denudation overlapped with final intrusion of the La Posta TTG (see also Kimbrough et al., 2001). Walawender et al. (1991), George and Dokka (1994), and others have proposed that tectonic denudation via normal faulting accompanied emplacement of the La Posta TTG. However, the extent to which the upper crust was extended in response to emplacement of the La Posta TTG may never be known since most of the affected rocks have been eroded away.

Biotite from positions east of the 85 Ma biotite K-Ar isochron record a second phase of rapid cooling with a distinctive early Laramide timing (i.e., beginning after ca. 80 Ma; Krummenacher et al., 1975). The rocks that record Late Campanian–Maastrictian Ar closure in biotite are structurally deeper than their western counterparts (Theodore, 1970; Gastil, 1979; Anderson, 1983; Engel and Schultejann, 1984; Grove, 1987; Ague and Brimhall, 1988; Todd et al., 1988; Rothstein and Manning, 2003). Major sedimentation is recorded along the western margin of the batholith at this time (Kennedy and Moore, 1971; Sundberg and Cooper, 1978; Nilsen and Abbott, 1981; Bottjer et al., 1982; Bottjer and Link, 1984; Fry et al., 1985; Girty, 1987; Bannon et al., 1989).

There is limited evidence for a final pulse of rapid cooling at the very end of the Cretaceous that appears to be restricted to the structurally deepest domains in the eastern batholith. These deep rocks, which cooled rapidly between 60 and 70 Ma (Krummenacher et al., 1975; Goodwin and Renne, 1991; Axen et al., 2000; Wenk et al., 2000), owe their exposure to either late cataclastic deformation along the eastern Peninsular Ranges mylonite zone and/or late Cenozoic extensional faulting within the Salton Trough and northern Gulf (Dokka and Merriam, 1982; Schultejann, 1984; Siem and Gastil, 1994; Axen and Fletcher, 1998). In any case, a mature erosion surface traversed by extra-regional depositional systems was developed throughout the northern Peninsular Ranges batholith by early Tertiary time (Kennedy and Moore, 1971; Peterson and Nordstrom, 1970; Abbott and Smith, 1978; Minch, 1979; Kies and Abbott, 1983; Abbott and Smith, 1989). Apatite fission track and (U-Th)–He data indicate that rocks of the eastern batholith still resided at several kilometers depth during the early Tertiary (Cerveny et al., 1991; Naeser et al., 1996; Wolf et al., 1997; Premo et al., 1998).

### Structural Breaks Coincident with the 85 Ma Biotite K-Ar Isochron

Krummenacher et al. (1975) have argued for a significant (~5 km) structural break between eastern and western lobes of the La Posta pluton on the basis of a sharp decrease of K-Ar biotite ages in the vicinity of Carrizo Gorge (Fig. 2). While this proposed structure would coincide approximately with the 85 Ma biotite K-Ar age contour, mapping in the Sweeny Pass 7.5′ quadrangle failed to reveal an important fault (Hoggatt, 1979). Less ambiguous evidence for a significant structural break near the surface expression along the 85 Ma isochron occurs between Cuyamaca Reservoir and Granite Mountain (Fig. 3).

The Chariot Canyon fault zone (Fig. 2; Kofron, 1984; Germinario, 1993; Grove, 1994) is a Late Cretaceous zone of top-to-the-west, ductile-to-brittle shear that coincides with a region of significant Late Cretaceous gold mineralization (Kofron, 1984). West of the Chariot Canyon fault zone, metamorphic grade recorded in pelitic intervals within Julian schist wallrocks increases from upper staurolite zone to sillimanite+K-feldspar zone toward the intrusive contact with the granodiorite of Cuyamaca Reservoir (Fig. 3; Grove, 1994). This metamorphic zonation was clearly developed in response to intrusion of the Cuyamaca Reservoir granodiorite during the middle Jurassic (Thomson and Girty, 1994; Murray and Girty, 1996). Shaw et al. (2003) report U-Pb zircon crystallization ages of 162–168 Ma for two samples of the Cuyamaca Reservoir granodiorite within the area of Figure 3. Garnet + biotite + andalusite + plagioclase + quartz thermobarometry performed with phyllitic rocks west of the Chariot Canyon fault zone indicate ~2.5–3.0 kbar conditions (Grove, 1994; see also Germinario, 1993). Steeply plunging isoclinal folds and lineations related to the Cuyamaca–Laguna Mountains shear zone are prevalent west of the Chariot Canyon fault zone.

The comparatively low-pressure western wallrocks are abruptly truncated against the Chariot Canyon fault zone (Fig. 3, Germinario, 1993; Grove, 1994). East of the Chariot Canyon fault zone, metamorphic grade is uniformly upper amphibolite facies (sillimanite-biotite-orthoclase gneiss) with migmatitic fabrics developed in appropriate bulk compositions regardless of proximity to intrusive contacts (Grove, 1987; see also Lampe, 1988). Petrogenetic relationships and garnet-biotite-$Al_2SiO_5$-plagioclase-quartz thermobarometry indicate 4.0–5.5 kbar conditions (Grove, 1987). Th-Pb dating of garnet-hosted monazite from one of the thermobarometry samples indicates that the upper amphibolite fabrics of the Granite Mountain area formed contemporaneously with intrusion of the La Posta pluton (M. Grove, unpublished ion microprobe data). While the ~1.5 kbar or roughly 5 km depth increase across the Chariot Canyon fault zone cannot be rigorously interpreted in terms of fault offset since peak grade assemblages on either side differ in age by ~70 m.y., the significant contrast in structural level across the zone (Fig. 3) can only be explained by large fault displacements.

Dominantly cataclastic deformation within the Chariot Canyon fault zone is superposed upon all synbatholithic structures, including well-developed secondary schistosity related to the Cuyamaca–Laguna Mountains shear zone that are developed in the granodiorite of Pine Valley in Oriflamme Canyon (Fig. 3; Thomson and Girty, 1994). The late deformation is characterized by lower greenschist facies recrystallization and ductile shearing along discrete, discontinuous zones of intense, brittle cataclasis (Fig. 3). Prehnite-actinolite facies assemblages (prehnite-epidote-chlorite-actinolite-albite-quartz in sheared tonalite) stable at 250–325 °C (Liou et al., 1987) are associated with the ductile fabrics: prehnite ± chlorite veins formed during the brittle cataclasis. Shallowly inclined, predominantly northwest-striking, northeast-dipping shear planes of cataclastic deformation (dark gray flinty gouge and ultracataclasite) are abundant both within and east of the Chariot Canyon fault zone. Indications of shear sense along these planes are conflicting but generally imply that the Chariot Canyon fault is a west-directed thrust or high-angle reverse fault (Grove, 1994). Although similar shear planes are present throughout the northeast region of Figure 2, they often exhibit normal geometry and appear to be related to Miocene extension (e.g., Schultejann, 1984). The Chariot Canyon fault zone was reactivated as an east-side down normal fault during the Late Cenozoic (Lampe, 1988).

### Cenozoic Deformation

Physiographically, the southwestern portion of the batholith shown in Figure 2 is an essentially intact structural block (Todd and Shaw, 1979). In contrast, the region northeast of the Elsinore fault has been noticeably affected by Late Cenozoic deformation. Vestigial, early Tertiary(?) erosion surfaces (e.g., Minch, 1979) preserved within topographically lower desert ranges northeast of the Elsinore fault generally occur at lower elevations than their southwestern counterparts. Because this implies net down-dropping of the desert ranges toward the Salton Trough, the regional northeastward increase in structural depth (e.g., Todd et al., 1988; Ague and Brimhall, 1988) cannot be an artifact of Cenozoic deformation. Middle Tertiary normal faults (Schultejann, 1984; Siem and Gastil, 1994; Axen and Fletcher, 1998; Lough and Stinson, 1991) have been described in a number of ranges northeast of the Elsinore fault. Many of these structures were formerly considered part of the Late Cretaceous eastern Peninsular Ranges mylonite zone (Sharp, 1979). With the exception of the normal fault system within the Sierra Cucupah and Sierra El Major (Siem and Gastil, 1994; Axen et al., 2000) ranges, Late Cenozoic normal faulting within the east-central Peninsular Ranges batholith near 33°N has produced a contrast in structural level that is barely resolved by apatite (U-Th)-He thermochronometry (Kairouz et al., 2003).

Late Cenozoic strike-slip faulting also does not appear to have greatly complicated the Late Cretaceous distribution of cooling ages within the area of Figure 2. While late Cenozoic strike-slip faulting has collectively displaced the main structural block of the batholith 25–40 km northwest relative to the easternmost desert ranges, most of this displacement has occurred

along the San Jacinto fault zone to the northeast of the area of Figure 2 (Sharp, 1967; Dorsey, 2002). While the Elsinore fault has accommodated up to 30 km of dextral offset at the northern end of the Peninsular Ranges batholith, much less displacement occurs within the area of Figure 2. Some of the displacement has been transferred further east to the Earthquake Valley fault and San Felipe faults (Magistrale and Rockwell, 1996). Along the Elsinore fault, displaced intrusive contacts limit right-lateral slip to less than ~2 km in the vicinity of Granite Mountain and Vallecito Valley (Fig. 3; Lampe, 1988; Todd et al., 1977a).

## METHODS

Granitic rocks were sampled at locations indicated in Figure 2. Sample selection was guided by the results of previous studies (e.g., Krummenacher et al., 1975). For reasons outlined in the introduction, a disproportionately large proportion of the samples were selected from positions that were anticipated to lie in close proximity to the estimated location of the 85 Ma biotite K-Ar isochron. Thermal history information was obtained from $^{40}Ar/^{39}Ar$ step-heating experiments performed using K-feldspar. Complementary $^{40}Ar/^{39}Ar$ results were also generated from coexisting hornblende, muscovite, and biotite. Argon isotopic analysis was performed at the University of California at Los Angeles using techniques and instrumentation discussed by Grove and Harrison (1996) and Quidelleur et al. (1997). Further details are provided in Appendix 1. Loss of radiogenic argon from hornblende and micas (i.e., total fusion ages) has been interpreted only in terms of bulk closure (e.g., Dodson, 1973) as constrained by hydrothermal argon diffusion experiments and/or well-constrained field settings (~525 °C for hornblende, ~400 °C for muscovite, and ~350 °C for biotite; see McDougall and Harrison, 1999). K-feldspar $^{40}Ar/^{39}Ar$ step-heating experiments, on the other hand, have been interpreted using the multi-diffusion domain approach (Lovera et al., 1989).

Our multi-diffusion domain (MDD) approach for recovering crustal thermal histories from $^{40}Ar/^{39}Ar$ step-heating experiments performed with K-feldspar is outlined in Lovera et al. (1997, 2002). The multi-diffusion domain character of K-feldspar appears to be related in poorly understood ways to the typically rich array of microstructures that typify basement feldspar (Lovera et al., 1993). Regardless of the nature of the intracrystalline controls, K-feldspar has been empirically demonstrated to be capable of recording continuous thermal history information from ~350 °C to ~150 °C (Lovera et al., 1997, 2002, and references cited therein; Parsons et al., 1999, offer a dissenting opinion). The extent to which samples we have examined are suitable for thermal history analysis is considered in greater detail in Appendix 2.

The age spectrum and Arrhenius data from a typical Peninsular Ranges batholith K-feldspar (AC) are shown in Figure 4A and Figure 4B respectively. One of the most significant sources of uncertainty involved in the estimation of thermal histories using the MDD approach is determination of activation energy ($E$). While $E$ is generally estimated from the slope defined by the

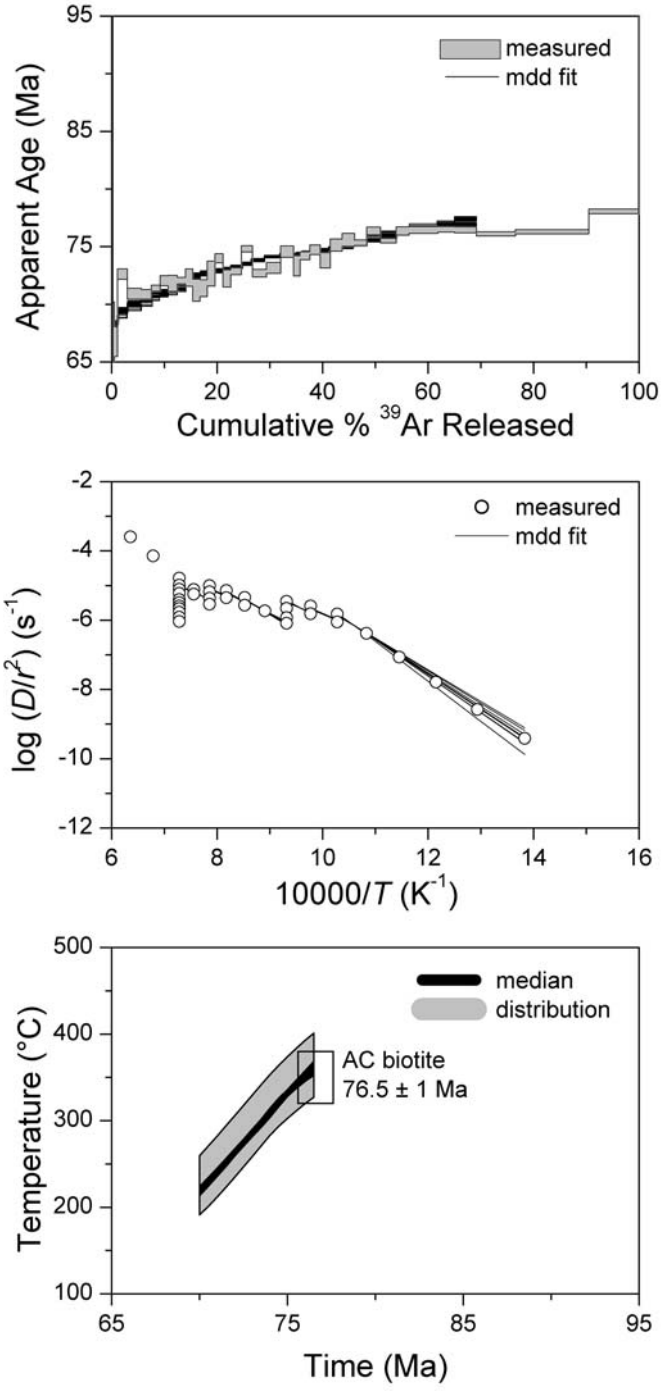


Figure 4. Representative K-feldspar thermal history results from AC K-feldspar. A: Age spectrum. Solid lines are 50 best-fit solutions from multi-diffusion domain thermal history analysis. B: Arrhenius plot. Solid lines represent 10 best-fit domain distributions obtained by allowing activation energy to vary by ± 3 kcal/mol about a mean imposed value of 46 kcal/mol (C) calculated thermal history. Envelopes indicate 90% confidence bounds for mean and overall distribution. See Table 2 for calculation limits and Appendix 2 for additional details of thermal history calculations.

initial low-temperature (~450–650 °C) data in the Arrhenius plot, the limited range over which the regression is performed may give rise to serious error in estimating this parameter. We have found the Arrhenius properties of Peninsular Ranges batholith K-feldspars to be remarkably similar. This has motivated us to employ a single fixed activation energy (46 kcal/mol) indicated by systematic analysis of several hundred K-feldspars (Lovera et al., 1997, 2002). To fit the Arrhenius data, we varied *E* within ± 3 kcal/mol limits to calculate 10 equivalent domain distributions (Fig. 4B). For each of these, five best-fit monotonically decreasing cooling histories were calculated to yield a total of 50 solutions. From these we determined the 90% confidence limits of the thermal history (Fig. 4C) that correspond to the interpreted portion of the age spectrum (i.e., the fraction of the $^{39}$Ar released below melting; see Fig. 4A).

## RESULTS

Our $^{40}$Ar/$^{39}$Ar results have been summarized in Table 1. Complete data tables are available in GSA's Data Repository[1]. Biotite and K-feldspar total gas ages have been plotted as a function of distance normal to the 85 Ma biotite age contour in Figure 5. Also included are previously published results from Armstrong and Suppe (1973) and Krummenacher et al. (1975) and new results from Ortega-Rivera (2003). These data define four domains (Fig. 5). Domain A in the southwest region of Figure 2 is characterized by variable biotite K-Ar ages between 95 and 110 Ma. An intermediate domain (= B) is defined by an ~15-km-wide expanse of comparatively constant 89–93 Ma ages. A second intermediate domain (= C) is defined by abruptly decreasing (1.3 m.y./km) biotite and K-feldspar total gas ages within ±5 km of the 85 Ma biotite isochron. The age gradient appears to be steepest (>2.5 m.y./km) across the Chariot Canyon fault zone (Chariot Canyon–Granite Mountain area; Fig. 3). Further north (Lake Henshaw-Ranchita area), the gradient is subtle (ca. 0.5 m.y./km). To the south, near the international border with México (Carrizo Gorge area; Fig. 2), the age gradient is about 1 m.y./km. The last northeastern domain (= D) defined by homogenous biotite K-Ar ages between ca. 80 and 75 Ma extends for at least 45 km to the east of the 85 Ma biotite isochron. Note that the youngest result (CM1) comes from the lower plate of a detachment fault system within the Coyote Mountains (Miller and Kato, 1991). In carrying out the more detailed K-feldspar thermal history analysis described below, we focus upon domains B, C, and D.

### K-Feldspar Thermal History Analysis

Details of the multi-diffusion domain modeling process are summarized in Table 2. Specific comments related to our ability to interpret the K-feldspar results are provided in Appendix 2. Interested readers are also directed to individual sample plots and model results that are available in GSA Data Repository (see footnote 1). Results of our thermal history calculations are summarized in Figure 6. We have also plotted (when available) thermal history estimates from biotite and muscovite total gas ages that assume 350 ± 30 °C and 400 ± 30 °C conditions for bulk closure respectively. To the extent possible, we have attempted to display the results in Figure 6 according to geographic position (see Fig. 2). Results obtained along the top row are from the northernmost samples arranged west to east and so forth. As stated in the "Methods" section, we represent the 50 best-fit thermal histories that were obtained for each sample by 90% confidence intervals for the median (black) and overall (gray) distribution. Note that we have permitted only monotonically decreasing cooling histories in our calculations.

From inspection of Figure 6 it is clear that all but the northernmost of samples (BM) from domain B had cooled to below ~200 °C by ca. 86 Ma. Apatite fission track results from domain B generally record cooling through ~125 °C by ca. 80 Ma (Naeser et al., 1996). Hence, slower cooling seems to be required for these samples subsequent to 86 Ma. Slower cooling subsequent to 86 Ma is recorded by most samples from domain C. Again, the northernmost samples from domain C record somewhat faster cooling between 86 and 78 Ma. Finally, all samples from domain D record rapid cooling from >350 °C conditions subsequent to about 78 Ma. Samples from the most easterly positions record the most rapid cooling. Apatite fission track results from this domain tend to yield 40–60 Ma ages (Naeser et al., 1996). This requires post–70 Ma deceleration of cooling rates throughout domain D.

Median cooling histories are plotted together in Figure 7A (note that we have omitted dissimilar results from the three northwest K-feldspar samples BM, SFH, and TS). These results are differentiated in Figure 7B to yield the Late Cretaceous cooling rates indicated by our calculations. The single bold curve in Figure 7B represents the mean cooling rate that is valid over most of the region outlined in Figure 2. Strictly speaking, the 95–86 Ma portion of this curve applies mainly to the western domain B rocks while the 78–65 Ma segment pertains primarily to the eastern domain D rocks. However, both independent apatite fission track data (Naeser et al., 1996) and results from domain C demonstrate that the later (78–68 Ma) phase of rapid cooling also must apply to domain B. Similarly, petrologic considerations and limited higher temperature thermochronologic constraints from hornblende and muscovite suggest that cooling rates in domain D must have been much slower prior to 78 Ma (i.e., these rocks existed at ~350–450 °C or about 11–15 km prior to 78 Ma, assuming a 30 °C/km geotherm).

In summary, it is clear that the east-central Peninsular Ranges batholith at 33°N experienced two phases of regionally extensive, Late Cretaceous rapid cooling. The first persisted from ca. 91 to 86 Ma and peaked at 88 Ma with a mean rate of ~25 °C/Ma. It overlapped with, and closely followed, emplacement of the La Posta TTG suite. We infer that it was primarily an expression of denudation that was triggered by massive

[1]GSA Data Repository Item 2003176, tabulated $^{40}$Ar/$^{39}$Ar analytical data, is available on request from Documents Secretary, GSA, P.O. Box 9140, Boulder, CO 80301-9140, USA, editing@geosociety.org, at www.geosociety.org/pubs/ft2003.htm, or on the CD-ROM accompanying this volume.

TABLE 1. $^{40}Ar/^{39}Ar$ RESULTS

| | Sample | Total gas age* | | | | Sample locations† | | Distance§ (km) | Description |
|---|---|---|---|---|---|---|---|---|---|
| | | Hbd (Ma) | Mus (Ma) | Bio. (Ma) | Ksp. (Ma) | Latitude | Longitude | | |
| 1 | 409-B | – | – | 78.6 | – | 32° 59.566’ | 116° 25.630’ | +8.56 | Gar-bio tonalite |
| 2 | 1110-I | – | 82.6 | – | 76.1 | 33° 02.396’ | 116° 24.426’ | +11.6 | Granite pegmatite |
| 3 | AC | – | – | 76.6 | 74.9 | 32° 55.896’ | 116° 16.450’ | +10.8 | La Posta tonalite |
| 4 | BM | – | – | 86.3 | 87.4 | 33° 12.901’ | 116° 42.477’ | –5.74 | Ranchita tonalite |
| 5 | BS | – | – | 87.1 | – | 32° 38.391’ | 116° 13.786’ | –3.6 | La Posta tonalite |
| 6 | BW-2 | – | – | – | 75.1 | 32° 50.222’ | 116° 14.765’ | +7.6 | La Posta tonalite |
| 7 | CAR | – | – | 81.0 | – | 32° 37.948’ | 116° 07.038’ | +6.6 | La Posta tonalite |
| 8 | CM-1 | – | – | – | 72.1 | 32° 47.266’ | 116° 01.231’ | +21.4 | Granodiorite |
| 9 | CP-175 | 100.1 | – | 84.8 | 80.8 | 32° 57.408’ | 116° 30.390’ | –1.2 | Gd. of Pine Valley |
| 10 | CP-128 | 101.1 | – | 91.9 | 92.7 | 32° 58.320’ | 116° 34.554’ | –5.9 | Gd. of Chiquita Peak |
| 11 | CS | – | – | 91.9 | 92.9 | 32° 56.401’ | 116° 33.880’ | –6.8 | Gd. of Chiquita Peak |
| 12 | CV | | – | 79.6 | 75.2 | 33° 12.689’ | 116° 26.592’ | +13.1 | Ranchita tonalite |
| 13 | DIA | – | – | 90.7 | – | 32° 42.290’ | 116° 21.983’ | –9.78 | La Posta tonalite |
| 14 | DSC | – | – | – | 91.1 | 32° 51.122’ | 116° 35.622’ | –15.0 | Granodiorite |
| 15 | EM | – | – | – | 91.9 | 32° 54.268’ | 116° 34.145’ | –9.7 | Granodiorite |
| 16 | EQ | 104.6 | – | 78.3 | – | 33° 00.827’ | 116° 23.467’ | +11.4 | Granite Mountain tonalite |
| 17 | EV | 101.9 | – | 84.0 | – | 33° 05.328’ | 116° 29.903’ | +4.1 | Granite Mountain tonalite |
| 18 | FCM | – | – | 78.4 | 76.4 | 33° 01.152’ | 116° 05.858’ | +29.6 | La Posta TTG tonalite |
| 19 | GM | 101.3 | – | 82.7 | 81.2 | 33° 03.061’ | 116° 28.784’ | +6.1 | Granite Mountain tonalite |
| 20 | IKPG | – | – | 77.6 | – | 32° 41.314’ | 116° 03.840’ | +13.0 | La Posta tonalite |
| 21 | IRR | – | – | 78.1 | – | 32° 38.948’ | 116° 06.616’ | +7.3 | La Posta tonalite |
| 22 | JU | 103.9 | – | 84.3 | 78.0 | 33° 01.105’ | 116° 31.694’ | +0.43 | Granite Mountain tonalite |
| 23 | JUCH | – | – | 89.4 | 91.5 | 33° 04.227’ | 116° 32.633’ | –4.7 | Granodiorite |
| 24 | KCR | – | – | 91.8 | – | 32° 43.272’ | 116° 28.315 | –17.5 | La Posta tonalite |
| 25 | KP | – | – | – | 91.6 | 32° 56.004’ | 116° 28.939’ | –1.2 | Harper Creek gneiss |
| 26 | LOS | – | – | 89.5 | – | 32° 40.617’ | 116° 19.852’ | –9.3 | La Posta tonalite |
| 27 | LBV-2B | – | 84.6 | – | 75.4 | 33° 01.521’ | 116° 25.964’ | +8.7 | Granite pegmatite |
| 28 | LP-80 | – | – | 90.3 | – | 32° 43.462’ | 116° 25.544 | –13.6 | La Posta tonalite |
| 29 | LPRR | – | – | 92.5 | – | 32° 38.686 | 116° 25.481 | –18.5 | La Posta tonalite |
| 30 | MMVT | – | – | – | 79.1 | 33° 04.292’ | 116° 32.455’ | +0.4 | Granite Mtn. tonalite |
| 31 | MP-17 | 108.8 | – | 90.2 | 85.7 | 32° 52.428’ | 116° 24.765’ | 0 | Las Blancas tonalite |
| 32 | MP | – | – | 80.7 | 76.5 | 32° 58.574’ | 116° 24.947’ | +6.3 | La Posta tonalite |
| 33 | MSR | – | 82.5 | 79.1 | – | 32° 40.225’ | 116° 06.352’ | +3.6 | La Posta tonalite |
| 34 | MVY | – | – | 91.2 | – | 32° 42.586 | 116° 23.063’ | –10.8 | La Posta tonalite |
| 35 | PV | – | – | 89.9 | 91.1 | 32° 48.798’ | 116° 30.644’ | –14.3 | Gd. of Pine Valley |
| 36 | RR | – | – | 88.9 | – | 33° 05.948’ | 116° 35.739’ | –4.6 | Cuyamaca Res. gd. |
| 37 | RG | – | – | – | 86.4 | 32° 58.322’ | 116° 30.956’ | –1.1 | Rattlesnake Gr. |
| 38 | SFH | 94.1 | – | 89.4 | 85.7 | 33° 13.082’ | 116° 34.673’ | +2.56 | Ranchita tonalite |
| 39 | SP | – | – | 76.7 | 75.3 | 33° 10.675’ | 116° 06.752’ | +41.3 | La Posta TTG tonalite |
| 40 | SY | 98.2 | – | 90.8 | 91.9 | 33° 05.895’ | 116° 39.850’ | –10.8 | granodiorite |
| 41 | TG | – | – | 79.4 | 78.9 | 33° 08.138’ | 116° 22.681’ | +15.9 | La Posta TTG tonalite |
| 42 | TS | | | 87.3 | 84.3 | 33° 12.554’ | 116° 36.251’ | +1.5 | Ranchita tonalite |
| 43 | WC | – | – | 83.7 | – | 32° 39.785’ | 116° 14.413’ | –3.2 | La Posta tonalite |
| 44 | WYN | – | – | 90.3 | – | 33° 05.670’ | 116° 37.851’ | –7.8 | granodiorite |
| 45 | YS | – | – | 78.9 | 74.8 | 33° 00.118’ | 116° 23.141’ | +10.9 | La Posta tonalite |

*Integrated $^{40}Ar/^{39}Ar$ ages. Internal precision is generally much smaller (<0.3%) than accuracy (±1.5%) based upon literature uncertainty in age of irradiation standard Fish Canyon sanidine (FCT-1). See text, Appendix 1, and the GSA Data Repository (see footnote 1) for additional details.

†Estimated from map positions.

§Distance normal 85 Ma biotite K-Ar age contour. The position of this curve was established from data in this study, Armstrong and Suppe (1972); Krummenacher et al. (1975); and Ortega-Rivera (this study).

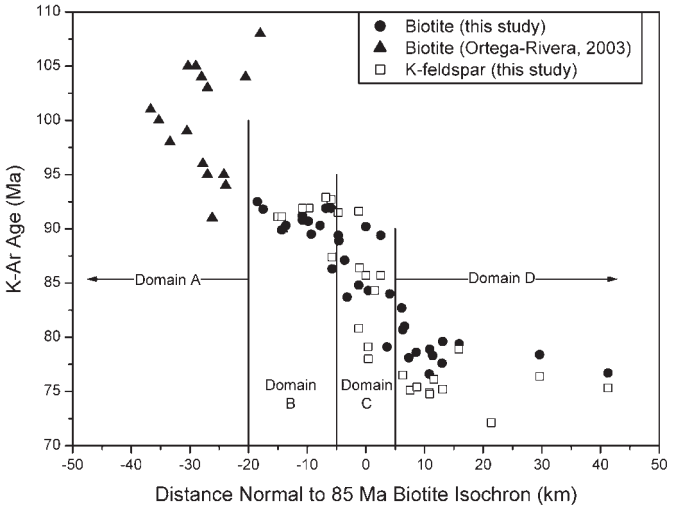


Figure 5. Biotite and K-feldspar total gas (= K-Ar) ages as function of distance (measured perpendicular to 85 Ma biotite K-Ar age isochron). Includes data from Armstrong and Suppe (1973), Krummenacher et al. (1975), and Ortega-Rivera (2003). Domains A, B, C, and D are discussed in text.

intrusion of the La Posta plutonic suite. In addition, the huge heat flux from the La Posta plutons must have significantly outgassed biotite and K-feldspar thermochronometers in their wallrocks. The second episode primarily affected the La Posta rocks ~20 m.y. after they were emplaced. While Krummenacher et al. (1975) originally recognized this relationship on the basis of mica bulk closure ages, the K-feldspar thermal history results presented here demonstrate it quantitatively with stark clarity. The event persisted from ca. 78 to 68 Ma and peaked at a mean rate of ~30 °C/Ma at ca. 73 Ma. More easterly rocks recorded far higher rates of cooling (to 80 °C/m.y.) over a shorter interval (76–72 Ma) centered around 74 Ma.

## DISCUSSION

Although the regional eastward decrease in K-Ar ages across the Peninsular Ranges batholith has been known for more than three decades (Everden and Kistler, 1970; Armstrong and Suppe, 1973; Krummenacher et al., 1975; Silver et al., 1979; Ortega-Rivera, 2003), the nature of the control(s) responsible for producing the pattern have remained uncertain. There is little doubt that when viewed at the scale of the entire southwestern margin of North America (e.g., fig. 17 in Ortega-Rivera, 2003), the regular eastward decline in age of K-Ar thermochronometers reflects multiple interacting processes such as magmatism, denudation, and subduction geometry that operate over broad regions (see also Ortega-Rivera, 2003). Hence, it is inescapable that conclusions drawn from small areas (e.g., Fig. 2) will fail to adequately explain complex behavior over the entire orogen. Nevertheless, it is only through such detailed studies that the true nature of the phenomenon can be incrementally understood.

TABLE 2. SUMMARY OF K-FELDSPAR MULTIDIFFUSION DOMAIN THERMAL HISTORY ANALYSIS

| Sample | MDD* | Interval of $^{39}$Ar release modeled | | Comments |
|---|---|---|---|---|
| | | Low-T limit† | High-T limit§ | |
| 1110-I | N | - | - | No MDD analysis |
| AC | Y | 3.0 | 69.2 | Inadequate temperature control |
| BM | Y | 0.6 | 31.3 | Interval of $^{39}$Ar release not extended with multiple 1100°C steps |
| BW-2 | Y | 1.3 | 76.1 | – |
| CM-1 | Y | 0.6 | 64.6 | Low-T misfit of age spectrum |
| CP-175 | Y | 0.2 | 85.0 | – |
| CP-128 | Y | 4.4 | 95.0 | – |
| CS | Y | 0.4 | 34.4 | Minor IAM resolved at 34.4% $^{39}$Ar |
| CV | Y | 0.4 | 77.3 | – |
| DSC | Y | 0.4 | 93.8 | – |
| EM | N | - | - | Inadequate temperature control |
| FCM | Y | 0.3 | 76.8 | – |
| GM | Y | 7.3 | 32.6 | Minor IAM resolved at 32.6% $^{39}$Ar |
| JU | Y | 1.4 | 90.6 | High uncertainties in age spectrum |
| JUCH | N | - | - | Inadequate temperature control |
| KP | Y | 0.6 | 42.2 | Appreciable IAM resolved at 42.2% $^{39}$Ar |
| LBV-2B | Y | 0.3 | 84.0 | – |
| MMVT | Y | 1.0 | 45.2 | Minor IAM resolved above 45.2% $^{39}$Ar |
| MP-17 | Y | 3.4 | 74.4 | - |
| MP | Y | 0.8 | 81.2 | High uncertainties in age spectrum |
| PV | N | - | - | Inadequate temperature control |
| RG | Y | 0.5 | 42.0 | Inordinately high low-Temp. $^{40}Ar_E$ |
| SFH | Y | 0.1 | 79.5 | – |
| SP | Y | 1.5 | 76.3 | – |
| SY | Y | 3.3 | 93.2 | – |
| TG | Y | 4.1 | 32.1 | Minor IAM resolved above 32.1% $^{39}$Ar |
| TS | Y | 0.1 | 44.6 | Interval of $^{39}$Ar release not extended with multiple 1100°C steps |
| YS | Y | 0.0 | 36.7 | Interval of $^{39}$Ar release not extended with multiple 1100°C steps |

*Note:* IAM refers to intermediate age maxima (see Appendix 2).

*MDD—multidiffusion domain thermal history analysis. Some samples were not analyzed due to poor temperature control.

†Lower limit of age spectrum modeled was determined by when evidence for fluid-inclusion hosted excess radiogenic $^{40}$Ar was no longer manifested.

§Upper limit established at final 1100 °C step (melting behavior is evident at high temperatures). Some samples exhibited problematic behavior at lower temperatures that further limited the interval of $^{39}$Ar release that we interpreted (see comment in adjoining column).

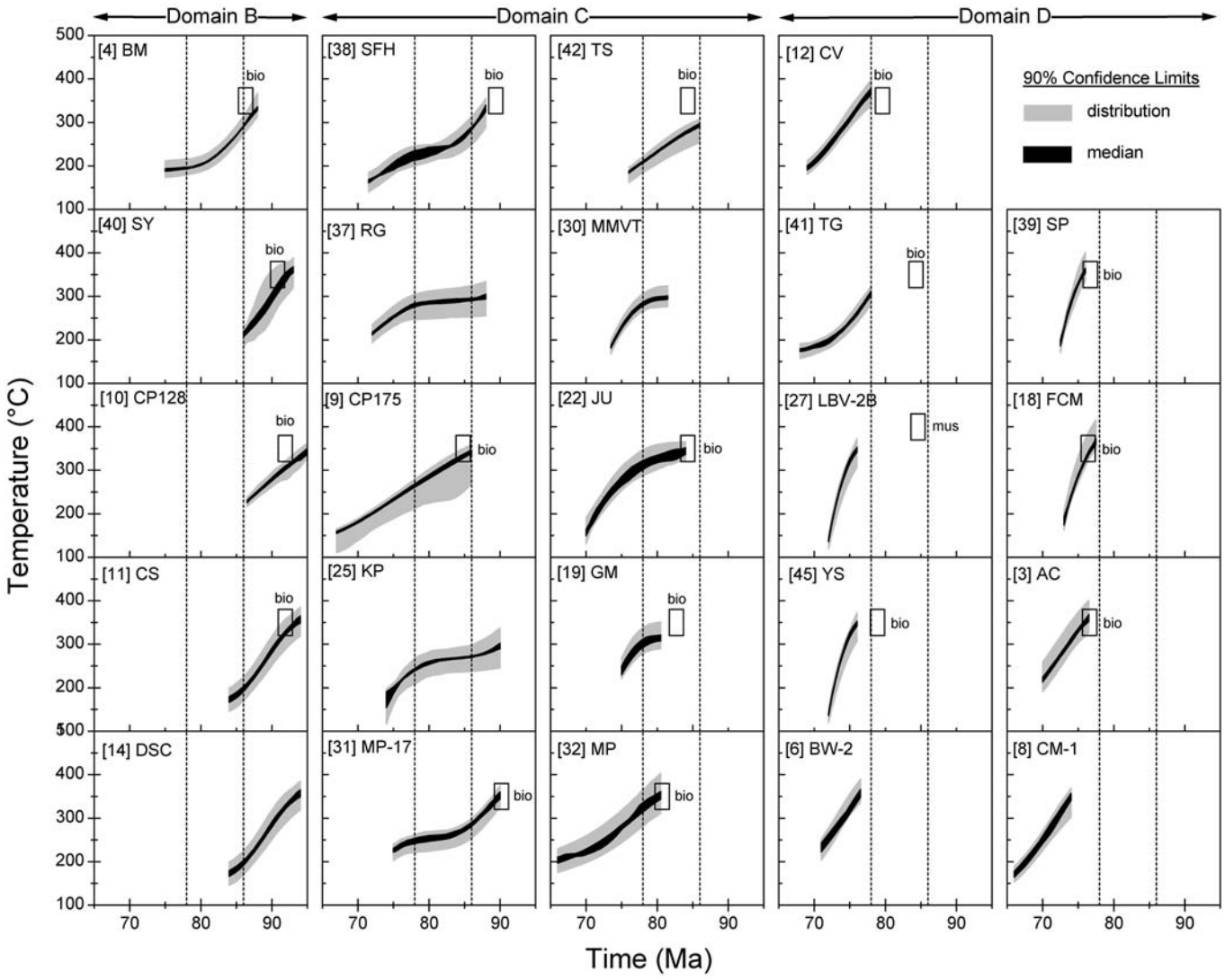


Figure 6: K-feldspar multi-diffusion domain (MDD) thermal history results from 24 K-feldspars from east-central Peninsular Ranges batholith. Confidence limits and age interval modeled for thermal history is same as in Figure 4. Domains B, C, and D are same as in Figure 5. Biotite (~350 ± 30 °C) and muscovite (400 ± 30 °C) bulk K-Ar closure after McDougall and Harrison (1999). See Table 2 and Appendix 2 for additional details.

Three principal schools of thought have arisen regarding the significance of the regional pattern of cooling ages within the northeastern Peninsular Ranges batholith. The first, articulated by Ortega-Rivera (2003), interprets the eastward decrease of cooling ages to fundamentally reflect a progressive eastward shift in magmatism. While such a view may be generally true for the western Cordillera (e.g., Coney and Reynolds, 1977), it provides an inadequate explanation for the east-central Peninsular Ranges batholith near 33°N where K-Ar ages postdate intrusion by as much as 10–20 m.y. The second view, favored by Krummenacher et al. (1975), among others, is motivated by the strong correlation between K-Ar age and erosion depth within the batholith and the coincidence of Late Campanian–Maastrictian rapid cooling with significant forearc sedimentation of this age. Proponents of this view interpret the timing of Late Cretaceous cooling as being dictated by when significant erosion denudation occurred. While this linkage is tantalizing, the late timing of the Late Campanian–Maastrictian cooling (10–20 m.y. after emplacement of the La Posta TTG suite) seems inconsistent with the expectation that arc crust should strengthen and increasingly resist deformation after intrusion has ceased.

A third school of thought, voiced by Dumitru et al. (1991), attributes the delayed cooling to the onset of Laramide shallow subduction (see Grove et al., 2003b). Late Cretaceous migration of the magmatic arc into the formerly adjacent regions of Sonora (Gastil and Krummenacher, 1977; Silver and Chappell, 1988; Staude and Barton, 2001; McDowell et al., 2001; Ortega-

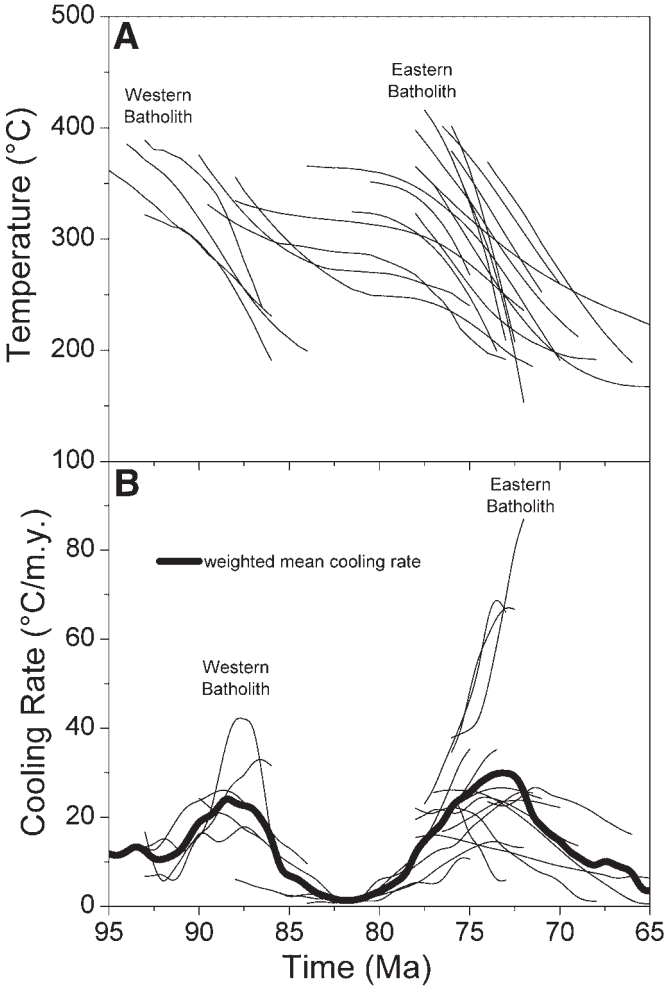


Figure 7. A: Summary plot of median K-feldspar cooling histories from Figure 6. Note that three results (BM, SFH, and TS from Lake Henshaw–Ranchita area) are somewhat different and have been omitted for clarity. B: Calculated cooling rates as function of time obtained by differentiating results in part A, above. Mean cooling history is indicated by bold curve.

Rivera, 2003) seemingly require that Laramide shallow subduction occurred beneath the Peninsular Ranges. Several previous studies have suggested that accelerated Late Cretaceous denudation was triggered by the onset of shallow Laramide subduction beneath the Peninsular Ranges batholith (George and Dokka, 1994; Grove, 1994). Dumitru (1990) and Dumitru et al. (1991) have interpreted Laramide timing of the cooling within the Sierra Nevada batholith in terms of heat flow from the overlying crust and mantle lithosphere into a shallowly subducting slab (subduction refrigeration). In their interpretation, K-Ar cooling ages directly reflect the timing of Laramide subduction and have little, if any, implication for when denudation occurred. In the following section, we evaluate both erosional denudation and subduction refrigeration with numerical models that are constrained by thermal history results from the east-central Peninsular Ranges batholith at 33°N.

## Numerical Analysis of Cooling Age Patterns

### *Cooling in Response to Erosional Denudation*

The simplest denudation process capable of reproducing the gross characteristics of the observed K-Ar cooling age patterns within the Peninsular Ranges batholith is hinged uplift or regional tilting (Ague and Brimhall, 1988; Butler et al., 1991; Ague and Brandon, 1992; Dickinson and Butler, 1998). Lovera et al. (1999) modeled the effects of overlapping intrusion (120–90 Ma) and hinged denudation (100–65 Ma) to interpret results from detrital thermochronometers from the Peninsular Ranges batholith forearc (see Appendix 3). Thermal histories of "eroded" material were determined by monitoring temperature variation throughout the grid. This information was used to calculate closure age distributions of detrital materials that could be compared with those measured from strata of known depositional age. Forward modeling of the detrital mineral age distributions permitted estimation of the batholiths erosional denudation history (see "Relationship to Forearc Sedimentation" section below).

While reasonably successful in reproducing detrital age distributions from the Peninsular Ranges batholith forearc, Lovera et al.'s (1999) model relied upon an overly simplistic representation of the distribution of erosion depth. The hinged denudation geometry they employed implied extremely deep erosion levels (>30 km) for formerly adjacent rocks in Sonora, México. In fact, available data indicate that erosion depth is more likely to have been symmetrically distributed about the east-central Peninsular Ranges batholith (Gastil, 1979). While Late Cenozoic formation of the Salton Trough and Gulf of California has obliterated key relationships, the Sonoran batholith on mainland México is known to expose shallow crustal levels and greenschist facies metamorphism (~1–3 km; Gastil and Krummenacher, 1977; Staude and Barton, 2001). Moreover, greenschist facies wallrocks that crop out in the Salton Trough (Coyote Mountains; Fig. 1) and Gulf of California (Sierra Pintas; Fig. 1) indicate that shallow erosion levels may also have been prevalent along the eastern margin of the Peninsular Ranges batholith (Gastil, 1979). Clearly, the deep (> 30 km) erosion depths implied for these regions by hinged denudation or regional tilting are inaccurate.

In this paper, we have modified the basement denudation model of Lovera et al. (1999) to permit a more symmetric distribution of erosion depth. We have constrained the denudation history with the new thermal history constraints presented in this paper and have extended the grid so that the shallow crustal levels and younger intrusion (90–65 Ma; see Anderson and Silver, 1974; Gastil and Krummenacher, 1977; Staude and Barton, 2001) within the Sonoran batholith on mainland México are represented. Interested readers are referred to Appendix 3 and Lovera et al. (1999) for further details.

Figure 8A illustrates the relevant portion of our calculation grid and shows the final distribution of K-feldspar bulk closure

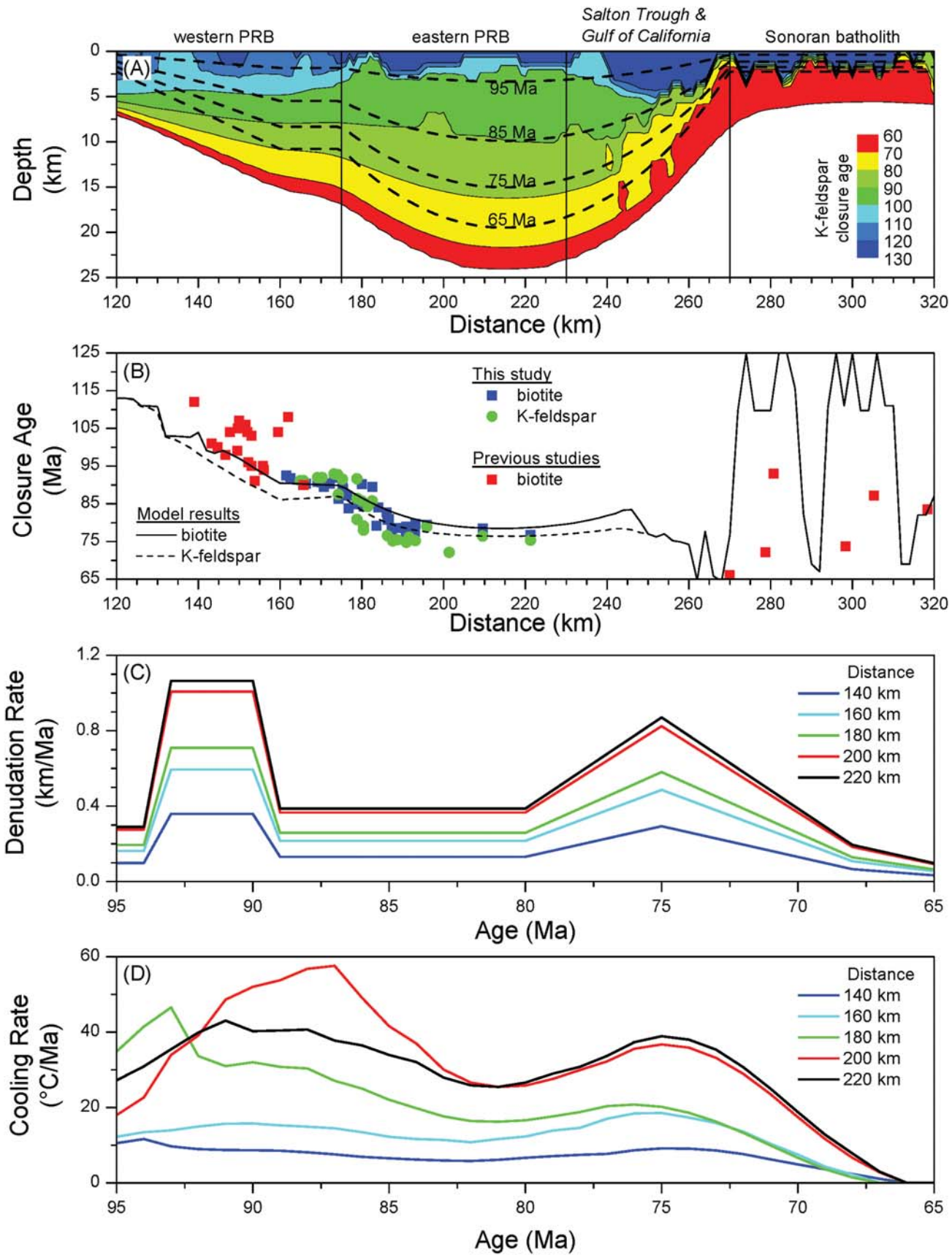


Figure 8. Results of erosional denudation calculations. A: Relevant portion of calculation grid showing contours of final K-feldspar closure ages used to calculate detrital age distributions in Figure 10. Positions of 95, 85, 75, and 65 Ma erosion surfaces are indicated by dashed lines. Irregularities in age contours are produced by transient heating during pluton emplacement. B: Predicted variation of biotite and K-feldspar K-Ar closure ages along final erosion surface in part A. C: Imposed denudation histories for different horizontal positions in grid as function of time. D: Calculated cooling rates for positions in C as function of time. Note that significant lag (~2–3 m.y.) exists between denudation and cooling during early denudation phase. PRB—Peninsular Ranges batholith.

ages produced by our numerical simulation of overlapping intrusion and erosional denudation (see Appendix 3 for additional details). It is important to realize that we simulated erosion by propagating surface temperatures (25 °C) into the grid. The position of the erosion surface at 95, 85, 75, and 65 Ma is represented by dashed lines in Figure 8A. Transient heating effects related to intrusion will be recorded at depths shallower than ~5–7 km beneath the active erosion surface (Lovera et al., 1999). At greater depths, K-feldspar is open to Ar diffusion, and the age distribution within the grid is controlled by denudation. For example, reheating effects related to 90–65 Ma pluton emplacement that are evident for grid positions between $240 < x < 260$ km at 10–20 km depths (i.e., within the region representing the Salton Trough and Gulf of California) were developed after significant denudation had occurred in this region.

The geometry of the final (i.e., 65 Ma) erosion surface in Figure 8A was constrained by the requirement that the available biotite and K-feldspar total gas ages of Figure 5 be reproduced (Fig. 8B). Several points bear mentioning. First, in the case of the Sonoran batholith and the western Peninsular Ranges batholith, we sought only to impose intrusive and denudation histories that simulated the first-order characteristics of these regions. We did not attempt to explicitly fit available data from these areas (Krummenacher et al., 1975; Gastil and Krummenacher, 1977; Ortega-Rivera, 2003) since they appear to reflect specific relationships to plutons that are not easily dealt with in our model. Second, the amount of denudation imposed upon the Salton Trough and Gulf of California region was based primarily upon extrapolation only. The intrusion history we imposed for this region was motivated in part by unpublished U-Pb zircon results from the Sierra El Major and Sierra Cucapa (Premo et al., 1998; Grove et al., 2003a). Finally, we failed to obtain a good numerical match to measured K-feldspar total gas ages from domain B from the east-central Peninsular Ranges batholith. K-feldspars from this domain tend to be slightly older than coexisting biotite; see Table 1 and Appendix 2). We believe this reflects a minor problem with excess $^{40}$Ar in the K-feldspars that we were unable to correct for (see Appendix 2). K-feldspars from domains C and D generally lack low-temperature excess $^{40}$Ar and yield total gas ages that are generally younger than those determined from biotite (Table 1).

Our calculations indicate erosion depths of about 11 km for domain B (Fig. 8A). An abrupt eastward increase in erosion depth beginning at $x = 175$ km coincides with the western limit of the eastern batholith. Note that the 85 Ma biotite age contour occurs at about $x = 185$ or 10 km east of the western boundary of the eastern batholith. This is compatible with the observed field relationship (Fig. 2). To the east of the 85 Ma contour, model K-feldspar total gas ages remain relatively constant. The maximum erosion depth we calculated for domain D occurs at $x = 215$ km. This value (20 km) corresponds to the upper limit of metamorphic pressures determined for the eastern Peninsular Ranges batholith (12–20 km; Grove, 1987; Ague and Brimhall, 1988; Todd et al., 1988; Rothstein and Manning, 2003). The assumed background geothermal gradient in our grid was 30 °C/km. Use of higher ambient geotherms would have reduced our estimates of erosion depth and vice versa.

In our calculations, we adjusted the denudation history (Fig. 8C) to obtain cooling histories (Fig. 8D) that were compatible with what we determined from our K-feldspar thermal history results (Fig. 7B). Comparison of Figure 8, parts C and D, reveals that there is a significant lag between the time of rapid denudation and the cooling that is produced by advective heat transport toward the surface. Because the early phase of denudation (93–90 Ma) overlaps with intrusion that ends at 90 Ma, transient heating has an impact on some of the solutions. In general, maxima in the cooling rates appear to be shifted by 2–3 m.y. relative to denudation rates with the greatest delays being recorded by the deepest rocks. An implication of this is that the cooling rate maxima we observe for our K-feldspars (at 88 Ma; see Fig. 7B) actually corresponds to maximum denudation at about 91 Ma. This adjustment would cause the timing of the earlier denudation pulse to be in better agreement with the 98–93 Ma interval for main phase emplacement of the La Posta TTG suite. In contrast, maxima in denudation and cooling both occur ca. 75 Ma during the later 80–68 Ma phase. Better agreement occurs because the rocks are closer to the surface when denudation starts.

### *Cooling in Response to Shallow Subduction*

Simple heat flow calculations performed by Dumitru (1990) involving a horizontal, instantaneously emplaced oceanic plate at very shallow (30–50 km) depths clearly demonstrated that large-scale crustal cooling of a former magmatic arc terrane would result from such a process. Here we present calculations of hanging wall thermal effects produced by a shallowly inclined, noninstantaneously emplaced oceanic plate using a geometry that we believe is more appropriate to the Peninsular Ranges batholith than the one adopted by Dumitru (1990). In our calculations, subduction initiates at 80 Ma (Fig. 9A). The slab has a 15° dip and is underthrust at 4 cm/yr. After 25 Ma of subduction, the thermal gradient within the calculation region has been reduced by a factor of two and a steady-state thermal structure has been approached (Fig. 9B). Cooling histories are presented for crustal depths of 5, 10, 15, and 20 km for both the left and right boundaries of the calculation region (Fig. 9C). Cooling produced by the shallowly subducting slab begins to occur within 1–3 m.y. after shallow subduction is initiated, depending upon its position within the area outlined in Figure 9B. Grid points near the left boundary experienced the most rapid cooling (10–50 °C/m.y., depending upon depth) with a peak at 76 Ma (Fig. 9D). Cooling rates are a factor of two lower (6–27 °C/Ma) along the right boundary with the peak occurring somewhat later (70–72 Ma, depending upon depth). Although we have not yet explored the effects of varying subduction parameters, it is clear that the timing and rates of cooling are comparable to those recorded by the eastern Peninsular Ranges batholith near 33°N (Fig. 7).

The calculated distribution of K-feldspar bulk closure ages for positions within the area outlined in Figure 9B is shown in

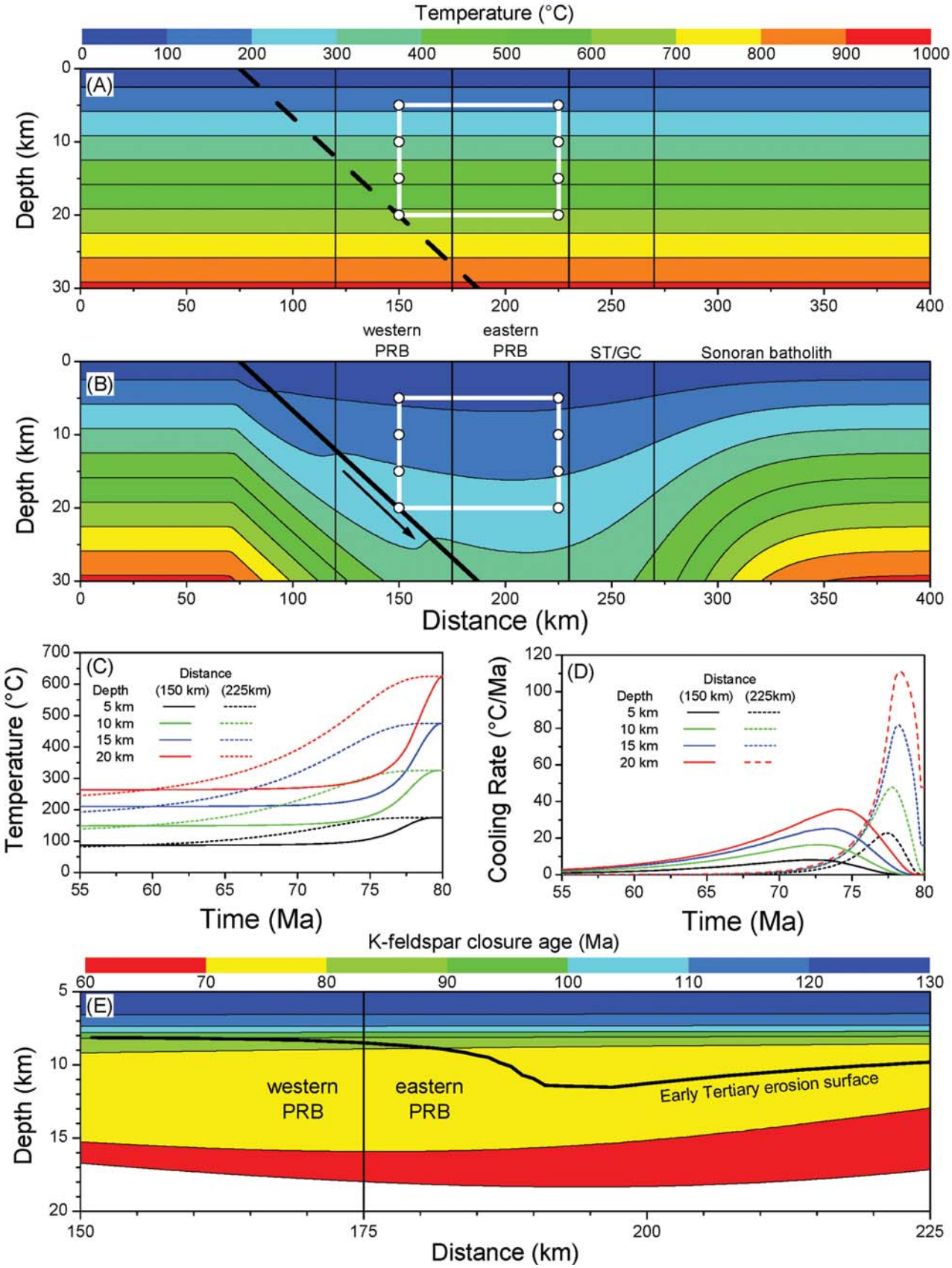


Figure 9. Calculation of hanging wall cooling (= subduction refrigeration) during shallow subduction. A: Initial geothermal structure at 80 Ma. Dashed bold line is future position of subducting oceanic plate (15° dip angle). Rectangular region indicates calculation points for panels C and D, below. Vertical lines indicate positions of western Peninsular Ranges batholith, eastern Peninsular Ranges batholith, Salton Trough/Gulf of California (ST/GC), and Sonoran batholith, respectively. B: Thermal structure developed by 55 Ma after 25 m.y. of 4 cm/yr underthrusting. C: Temperature-time histories at eight calculation points illustrated in panel A, above. D: Cooling histories for same calculation points. E: Distribution of K-feldspar bulk closure ages at 55 Ma. Bold line indicates position of erosion surface that corresponds to closure age profile of Figure 5. Erosion down to this surface must take place during continued steady-state underthrusting. Under these conditions, magnitude of erosional denudation is roughly half of that required in absence of subduction refrigeration (compare with Fig. 8A).

Figure 9E. Note that the subnormal geothermal gradients produced by subduction refrigeration cause K-feldspar to experience bulk Ar closure over a much broader region (and to significantly greater depths) than is the case when rocks cool solely due to proximity to the surface. As a result, the depths implied by the data in Figure 5 are only half as deep as those deduced from the erosion denudation model (compare Figs. 8A and 9E). Calculation of this surface assumes erosion occurs under near steady-state conditions of shallow subduction. However, note that the maximum depth attained (11 km) is at the lower limit estimates of metamorphic depth for portions of the eastern batholith that lie east of the 85 Ma biotite age contour (12–20 km; Grove, 1987; Ague and Brimhall, 1988; Todd et al., 1988; Rothstein and Manning, 2003). In addition, because lateral thermal gradients are greatly subdued, the steep age gradient that occurs in the vicinity of the 85 Ma biotite isochron requires a more abrupt depth increase than is the case for erosion denudation (compare Fig. 8A with Fig. 9D). Such an abrupt transition can only be explained by east-side-up faulting.

**Relationship to Forearc Sedimentation**

As demonstrated in the previous section, erosional denudation and subduction refrigeration mechanisms imply significantly different erosion depths for the east-central Peninsular Ranges batholith at 33°N. In the subduction refrigeration model, erosion can significantly postdate cooling without leaving a signal resolvable by biotite and K-feldspar thermochronometers provided that the low geothermal gradient produced by shallow subduction is maintained indefinitely. Alternatively, the erosion denudation model predicts that significant sedimentation will correlate strongly with major cooling events in the batholith. Because of this, the erosion denudation model can be further tested by determining how well it accounts for the age distributions of detrital thermochronometers in the forearc (Fig. 10).

Lovera et al. (1999) determined that it was possible to deduce important aspects of basement denudation histories from detrital thermochronometers. In their analysis of materials from the northern Peninsular Ranges batholith forearc (Santa Ana mountains and La Jolla; see locations in Fig. 1), they determined that a constant mean denudation rate of 0.5 mm/yr from 100–65 Ma fit the detrital K-feldspar K-Ar results reasonably well and that a 0.25 mm/yr rate was too slow. In refining their calculations, Lovera et al. (1999) concluded that the best fit to the data involved initially rapid erosion following emplacement of the La Posta TTG during the Cenomanian–Turonian (92–89 Ma; 1.25 mm/yr; Fig. 11A). They also found that erosion rates had to decrease during the Santonian–early Campanian (0.15 mm/yr from 89 to 78 Ma;) to match detrital results from this interval. Finally, a second accelerated phase was indicated by results from Late Campanian–Early Maastrictian sediments (0.45 mm/yr beginning at 78 Ma). We find it remarkable that the erosion denudation history implied by our basement thermal history results so well matches that determined independently from forearc strata (Fig. 11B). Note that the constant denudation shown after 73 Ma in the Lovera et al. (1999) result is not constrained by data they obtained from the forearc sediments.

To further explore the compatibility of the two independent data sets, we have calculated detrital K-feldspar closure age distributions from our revised erosion denudation model. Because we consider it unlikely that drainage systems would have extended completely across the actively denuding region of Figure 8A, we established a drainage divide at the inferred eastern limit of the Peninsular Ranges batholith (at $x$ = 230 km). The broad similarity in the measured and calculated age distributions that we obtained indicates that the overall magnitude and timing of basement denudation that we imposed in the calculations is well calibrated (Fig. 10, Table 3). This is an important point since denudation that is too fast or too slow can dramatically shift calculated detrital age distributions (see Lovera et al., 1999). Even so, Kolmogorov-Smirnoff analysis of the measured and synthetic data sets (see Lovera et al., 1999) reveals that the model age distributions are not as similar to the measured distributions as they could be (Table 3). Specifically, the well-defined maxima evident in our calculated spectra are not expressed in the detrital K-feldspar age distributions measured from the forearc (Fig. 10). Our model produces strong peaks in the detrital age distributions when material from the deeply denuded east-central Peninsular Ranges batholith predominates over other sources (Fig. 8A). As indicated in Figure 8A, western zone rocks yield a more dispersed distribution of bulk closure ages by virtue of their derivation from shallower levels. Based upon these results it seems clear that while our erosion denudation model for the Peninsular Ranges batholith is in reasonable agreement with the forearc results, there is need for further revision.

There are at least two potentially important factors that could cause shallower western zone rocks to be overrepresented in detrital age distributions sampled from the forearc. First, K-feldspar is less prevalent in the eastern batholith because it is dominated by the La Posta TTG suite (Baird and Miesch, 1984). Hence, K-feldspar will be disproportionately derived from the western batholith. If we were to weight our model results with respect to the abundance of $K_2O$, as constrained by Baird and Miesch's (1984) data set, K-feldspar yields from western zone rocks would be significantly increased. Second, the sedimentary sequences sampled by Lovera et al. (1999) onlap the batholith and could therefore receive an enhanced sediment load from local western sources. More distal forearc strata to be sampled in the future should be more representative of the batholith as a whole.

**Extent of Faulting**

Our present calculations do not explicitly consider the role of faulting in denuding the Peninsular Ranges batholith. A number of authors (Krummenacher et al., 1975; Goodwin and Renne, 1991; George and Dokka, 1994; Grove, 1994; Ortega-Rivera et al., 1997; Ortega-Rivera, 2003) have argued that faults with large

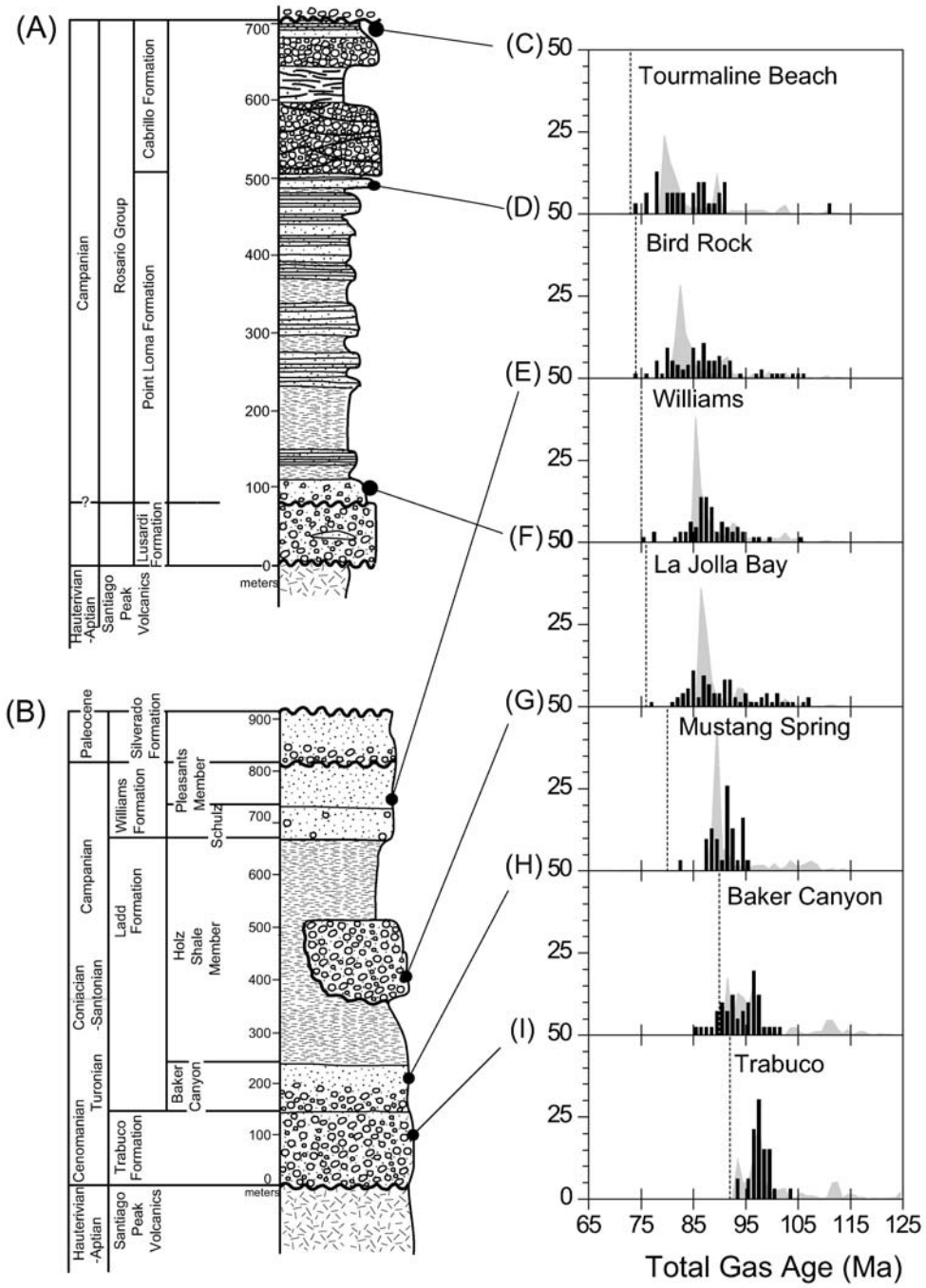


Figure 10. Stratigraphy of Peninsular Ranges batholith forearc strata (localities shown in Fig. 1A). A: La Jolla area. B: Northern Santa Ana Mountains. C–I: Solid (black) histograms represent measured detrital K-feldspar $^{40}Ar/^{39}Ar$ closure age distributions for stratigraphic positions located in panels A and B. Dashed vertical lines indicate depositional age (see Lovera et al., 1999). Gray curves represent calculated detrital K-feldspar distributions from data of Figure 8A. Overall similarity of measured and calculated age distributions indicates that Peninsular Ranges batholith denudation history is well calibrated. Additional details about good fit are presented in Table 3.

vertical components of displacement were locally significant in influencing K-Ar age gradients within the northeastern Peninsular Ranges batholith. The most obvious Late Cretaceous structure to affect the batholith is the west-vergent eastern Peninsular Ranges mylonite zone (Sharp, 1979; Simpson, 1984; Engel and Schultejann, 1984). While high-temperature mylonitization along this zone (e.g., Theodore, 1970) appears to have been largely coeval with emplacement of the La Posta TTG (Todd et al., 1988), continued, Late Cretaceous cataclastic deformation along the eastern Peninsular Ranges mylonite zone has been documented by Goodwin and Renne (1991) and Wenk et al. (2000) in the San Jacinto and Santa Rosa mountains.

The rocks that we are considering from the east-central Peninsular Ranges batholith near 33°N are all situated southwest of the eastern Peninsular Ranges mylonite zone (Fig. 1). Cataclastic deformation similar to that developed within the eastern Peninsular Ranges mylonite zone occurs but is associated with more subtle structures. Of these, the Chariot Canyon fault zone is the most

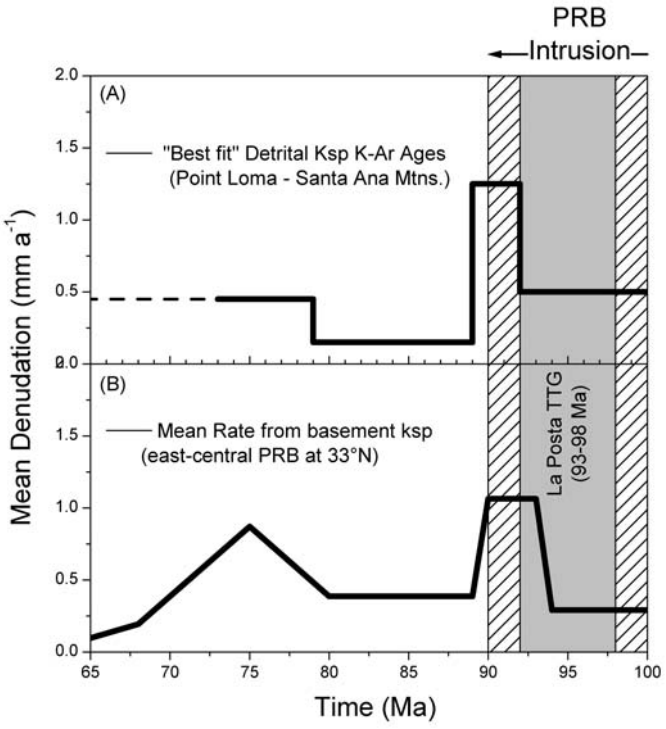


Figure 11. A: Erosional denudation histories deduced from detrital K-feldspars from northern Peninsular Ranges batholith forearc (Lovera et al., 1999). Dashed segment is not constrained by detrital data. B: Erosional denudation histories deduced from basement K-feldspars from east-central Peninsular Ranges batholith near 33°N. Gray region in A and B above represents emplacement interval for La Posta TTG (tonalite-trondhjemite-granodiorite) suite after Kimbrough et al. (2001). Hatched region indicates limits of meaningful intrusion within east-central Peninsular Ranges batholith at 33°N after Silver and Chappell (1988), Walawender et al. (1990, 1991), and Lovera et al. (1999).

TABLE 3. COMPARISON OF MEASURED AND MODEL DETRITAL K-FELDSPAR CLOSURE AGE DISTRIBUTIONS

| Sample | Lovera et al. (1999) | | This study | |
|---|---|---|---|---|
| | $\Delta t^*$ (Ma) | Log $PROB_{MAX}$ | $\Delta t^*$ (Ma) | Log $PROB_{MAX}$ |
| Trabuco | 0 | –2.3 | 0 | –2.3 |
| Baker Canyon | 0 | –1.8 | 0 | –2.1 |
| Mustang Spring | 0 | –1.8 | 0 | –1.7 |
| La Jolla Bay | 0 | –2.6 | 0 | –4.3 |
| Williams | +1 | –0.8 | 0 | –2.0 |
| Bird Rock | +1 | –0.2 | –1 | –3.2 |
| Tourmaline Beach | +1 | –0.2 | –2 | –1.0 |

*$\Delta t$—difference between the best fit erosion surface predicted by the model and the independently determined depositional age for the sample (see Lovera et al., 1999).

†$PROB_{MAX}$—Kolmogorov-Smirnov statistic (Press et al., 1986) obtained from comparison of best-fit closure age distribution obtained from model and detrital K-feldspar $^{40}Ar/^{39}Ar$ closure age distribution measured from sample (see Lovera et al., 1999).

obvious example (Fig. 3). Our K-feldspar thermal history results record a 150°C temperature difference across it prior to 78 Ma (Fig. 7). This corresponds to ~5 km vertical separation assuming a 30 °C/km geotherm. By about 68 Ma, rocks positioned east of the Chariot Canyon fault zone had cooled substantially (Fig. 7). Well-developed, early Tertiary(?) erosion surfaces developed on either side of the Chariot Canyon fault zone differ in elevation by less than 650 m. Because the erosion surfaces are actually dropped down to the east in a sense that is compatible with extensional faulting associated with Late Tertiary formation of the Salton Trough (Lampe, 1988), it seems clear that formation of the erosion surfaces post-dated earlier east-side-up displacement along the Chariot Canyon fault zone.

Elsewhere, it is difficult to prove that faulting has influenced cooling age patterns. Krummenacher et al. (1975) argued that the La Posta pluton was offset by an east-side-up fault displacement on the basis of a sharp decrease of K-Ar biotite ages in the vicinity of Carrizo Gorge (Fig. 2). While this proposed structure would coincide approximately with the 85 Ma biotite K-Ar age contour, mapping in the Sweeny Pass 7.5′ quadrangle failed to reveal an important fault (Hoggatt, 1979).

Conclusions based upon our numerical analysis of erosional denudation would need to be re-evaluated if additional work demonstrated that Late Cretaceous tectonic denudation via normal faulting played a major role in the Late Cretaceous evolution of the east-central Peninsular Ranges batholith near 33°N. Currently there is little evidence that this was an important factor. Normal faults of potential Late Cretaceous age were mapped by Erskine and Wenk (1985) in the San Jacinto and Santa Rosa Mountains. Cataclastic deformation along minor low-angle fault surface occurs sporadically throughout the east-central Peninsular Ranges batholith near 33°N (Ratschbacher and Grove, unpubl. mapping). Some or all of these structures may be late Tertiary in age and similar to normal fault systems developed at Yaqui Ridge and the Vallecito Mountains (Schutejann, 1984; Lough and Stinson, 1991), the Coyote Mountains (Miller and Kato, 1991), and the Sierra El Major and Sierra Cucapá (Siem and Gastil, 1994; Axen and Fletcher, 1998; Axen et al., 2000). The only normal faults that are known to have exposed significantly deeper rocks in their footwalls are Late Miocene–Pliocene structures that occur within the Sierra El Major and Sierra Cucapá (Axen et al., 2000).

## Driving Mechanisms for Late Cretaceous Denudation

It seems clear that early Late Cretaceous denudation (centered around 91 Ma; see Figs. 7B and 8C and D) is most simply explained as a consequence of massive intrusion of the eastern Peninsular Ranges batholith by the 96 ± 3 Ma La Posta TTG suite (see also Kimbrough et al., 2001). While more ambiguous, we believe that the driving mechanism(s) behind the later (i.e.,

< 78 Ma) cooling was most likely erosional denudation related to Laramide shallow subduction (Coney and Reynolds, 1977; Dickinson and Snyder, 1978; Bird, 1988). Subduction refrigeration may also have played a role. We speculate that the eastern Peninsular Ranges batholith lithosphere was eroded up to the base of the lower crust during Laramide shallow subduction beginning ca. 80 Ma and that removal of this material destabilized the overlying crust and triggered erosion and localized shortening along features such as the Chariot Canyon fault zone to restore the density balance between the crust and the upper mantle. Regional development of erosional surfaces and extraregional depositional systems across the Peninsular Ranges batholith (Minch, 1979; Kies and Abbott, 1983) signal that these processes had run their course by latest Cretaceous–early Tertiary time.

## CONCLUSIONS

We draw the following conclusions for the thermal evolution of the east-central Peninsular Ranges batholith near 33°N:

1. The 85 Ma biotite K-Ar age isochron delineates rocks that have experienced contrasting cooling histories. We recognize four domains. At >20 km southwest of the 85 Ma contour, biotite $^{40}Ar/^{39}Ar$ total gas (= K-Ar) ages are old (>95 Ma) and variable. From 5 to 20 km southwest of the 85 Ma isochron, biotite and K-feldspar ages are 90–93 Ma. Within ± 5 km of the 85 Ma isochron, biotite and K-feldspar ages drop sharply to the east by about 1.3 m.y./km). As much as 40 km northeast of the 85 Ma isochron, biotite and K-feldspar ages are 74–77 Ma over a broad area (>3000 km$^2$).

2. Multi-diffusion domain thermal history analysis of K-feldspar permits us to clearly resolve two phases of rapid cooling. The first episode is recorded primarily by rocks positioned west of the 85 Ma isochron. It persisted from ca. 91–86 Ma and peaked at 88 Ma with a mean rate of ~25 °C/m.y. Our numerical model of erosional denudation indicates a lag between denudation and cooling of ~3 m.y. Hence, peak cooling at 88 Ma corresponds to peak denudation at 91 Ma.

3. The second episode of rapid cooling was recorded mainly by rocks east of the 85 Ma contour. The event persisted from ca. 78–68 Ma and peaked at a mean rate of ~30 °C/Ma ca. 73 Ma. More easterly rocks recorded far higher rates of cooling (to 80 °C/Ma) over a shorter interval (76–72 Ma) centered around 74 Ma. Rocks in close proximity to the 85 Ma contour tend to record both cooling phases as well as slower cooling between 86–78 Ma.

4. A locally sharp K-Ar age gradient across the 85 Ma isochron (up to 2.5 m.y./km) in the vicinity of the Chariot Canyon fault reflects ductile to brittle, east-side-up shearing along it. Elsewhere along the 85 Ma isochron, field evidence for Late Cretaceous faulting is lacking.

5. Numerical analysis of erosion denudation indicates that our thermal history results can be largely explained by rapid denudation (up to 1 mm/yr) in two phases from 93 to 90 Ma and from 80 to 68 Ma. Erosion depths predicted from this model (up to 20 km) are near the upper limits of thermobarometric estimates from the eastern batholith.

6. Numerical analysis of cooling effects produced immediately above shallowly inclined (~15°) subduction zones (subduction refrigeration) indicates that the latter can also account for the later rapid cooling in the eastern Peninsular Ranges batholith if 4 cm/yr underthrusting is initiated at 80 Ma. Erosion depths predicted by this model (up to 11 km) are a factor of two lower than those estimated in the absence of subduction refrigeration and are at the lower limit of thermobarometric estimates for the eastern batholith.

7. Erosional denudation histories deduced for the northern Peninsular Ranges batholith using independent means (basement sampling and analysis of forearc sediments) yield remarkably similar results and indicate that erosional denudation was the most important factor in producing both episodes of Late Cretaceous cooling.

8. We believe that the early denudation phase (~93–90 Ma) was related to massive intrusion of the batholith by the La Posta TTG suite. Later 80–68 Ma denudation may have occurred in response to removal of the lower crust and underlying lithospheric mantle during Laramide shallow subduction.

## APPENDIX 1: $^{40}AR/^{39}AR$ ANALYSIS DETAILS

Hand-selected muscovite and biotite (~5 mg) and hornblende (~25 mg) were wrapped in Sn foil and packed along with Al-wrapped Fish Canyon sanidine (FCT-1: 27.8 ± 0.3 Ma) flux monitors in 6 mm ID quartz tubes that were evacuated and sealed. Fe–mica biotite (307.3 Ma) was used to monitor K-feldspar samples (~200 mg) that were similarly packaged for irradiation. See Grove and Harrison (1996) for additional information regarding the Fe–mica biotite standard. Samples were irradiated at the University of Michigan's Ford reactor (L67 position). See McDougall and Harrison (1999) for more information regarding this facility and $^{40}Ar/^{39}Ar$ irradiation procedures. Correction factors for reactor-produced K- and Ca-derived argon were determined by measuring $K_2SO_4$ and $CaF_2$ salts included with each irradiation. Because several irradiations were performed, it is inefficient to include further information here. Instead, we provide data reduction parameters relevant to each sample in their respective data tables in the data repositiory. This information includes irradiation history, the date of $^{40}Ar/^{39}Ar$ analysis, and all irradiation parameters (J, $^{40}Ar/^{39}Ar_K$, $^{38}Ar/^{39}Ar_K$, $^{36}Ar/^{37}Ar_{Ca,}$ and $^{39}Ar/^{37}Ar_{Ca}$).

Most K-feldspar samples were incrementally heated in a double vacuum Ta furnace (see Lovera et al., 1997, for additional information regarding K-feldspar step-heating experiments). Evolved gas was transferred with the aid of liquid nitrogen-activated charcoal and purified with a SAES ST-101 50 l/s getter pump. $^{40}Ar/^{39}Ar$ measurements were performed with an automated Nuclide 4.5–60-RSS mass spectrometer that was equipped with a Nier source and a Faraday detector, and it was typically operated at an Ar sensitivity of $1.5 \times 10^{-15}$ mol/mV. Gas was admitted to the mass spectrometer with the aid of a leak valve to ensure that the quantity of gas analyzed did not exceed the linear range of the detection system. Orifice corrections were performed where necessary. Values of $^{39}Ar$ have been normalized to 100% gas delivery to the mass spectrometer. Fe–mica biotite flux monitors packed with the K-feldspars were analyzed following similar techniques. Additional experimental details are presented in Grove and Harrison (1996).

Three of the K-feldspars and all of the hornblende and muscovite samples were analyzed with a VG1200S mass spectrometer. This

instrument is equipped with a Baur-Signer source and an electron multiplier and was operated at a sensitivity of $4 \times 10^{-17}$ mol/mV. Evolved gas was transferred by expansion and purified with a SAES ST-101 10 l/s getter pump. Gas delivery to the mass spectrometer was governed by splitting using calibrated procedures.

Biotite samples were fused with a Coherent 5 W Argon ion laser and analyzed with a VG3600 mass spectrometer. This instrument was equipped with a "bright" Nier source and a Daly photomultiplier and was operated at an Ar sensitivity of $2 \times 10^{-17}$ mol/mV. Generally each analysis entailed fusion of ~five 40–60 mesh grains. The extraction line and procedures were similar to those of the VG1200S. Additional details about both of these extraction line/mass spectrometer systems are provided in Quidelleur et al. (1997).

Intercalibration studies of different splits of FCT-1 sanidine involving the VG1200S and VG3600 extraction lines revealed no statistically significant (<0.3%) difference between either instrument (their pipette systems were filled simultaneously from a common aliquot of atmospheric Ar). J-factors calculated from Fe–mica biotite on the nuclide were generally agreed with splits run on the VG1200S to less than 0.5%. When J-factors calculated from adjacently packaged FCT-1 sanidine and Fe–Mica biotite were run on the VG1200S, they also agreed to within 0.5% (Fe–Mica biotite was systematically high). The error in age implied by this potential miscalibration of FCT-1 sanidine and Fe–Mica biotite for Late Cretaceous samples is less than 0.5 Ma.

Values $^{40}Ar/^{39}Ar$, $^{38}Ar/^{39}Ar$, $^{37}Ar/^{39}Ar$, and $^{36}Ar/^{39}Ar$ listed in data tables were corrected for total system backgrounds, mass discrimination (monitored by measurement of atmospheric Ar introduced by a pipette system), abundance sensitivity, and radioactive decay. Correction of $^{40}Ar/^{39}Ar$ ratios for nuclear interferences and atmospheric argon and calculation of apparent ages was carried out as described in McDougall and Harrison (1999) using conventional decay constants and isotopic abundances Steiger and Jäger (1977). Additional information is provided in footnote form with the data tables.

## APPENDIX 2: DETAILS OF K-FELDSPAR MDD THERMAL HISTORY ANALYSIS

The principal requirement for successful application of the MDD approach is that thermally activated release of reactor-induced $^{39}Ar$ during laboratory step-heating experiments adequately portrays diffusion of radiogenic $^{40}Ar$ in nature (i.e., the same diffusion mechanisms and boundaries control Ar transport in both cases). This requirement cannot be met if volumetrically significant recrystallization occurs subsequent to the onset of radiogenic argon ($^{40}Ar^{*}$) retention at ~300–350 °C (Lovera et al., 2002; see also Parsons et al., 1999). Such an assessment can be made by assessing the extent of correlation between $^{39}Ar$ and $^{40}Ar/^{39}Ar$ spectra (Lovera et al., 2002). The age spectrum reflects millions of years of Ar transport in nature while the $^{39}Ar$ diffusion properties image this behavior over minutes to hours at elevated temperatures in the laboratory. If both reflect the same intrinsic process and boundaries for Ar transport, then the two spectra should be highly correlated (Lovera et al., 2002). The fact that K-feldspars examined in this study exhibit generally high correlation between nucleogenic ($^{39}Ar$) and radiogenic ($^{40}Ar$) argon (typically >0.9) is strong evidence that natural diffusion properties have been reproduced in the laboratory with reasonably high fidelity.

Calculations were performed for 24 of 28 K-feldspars. Step-heating results from samples 1110-I, EM, PV, and JUCH were not interpreted due to highly imprecise temperature control. Based upon the similarity of their age spectra to those of adjacent samples, however, we believe it is likely that they would have yielded compatible results. A first-order expectation of volume diffusion in a multi-diffusion domain sample is that the age spectrum should increase monotonically. Nearly all K-feldspars we have examined (e.g., Lovera et al., 2002) exhibited evidence of minor low-temperature $^{40}Ar_E$ contamination that we believe to have originated from decrepitating fluid inclusions (Harrison et al., 1994). Evidence for this generally subsided between 600 and 700 °C. For samples that also exhibit signs of high-temperature $^{40}Ar_E$ contamination, evidence for this (i.e., erratic age variation that is uncorrelated with $^{39}Ar$ diffusion properties; see McDougall and Harrison, 1999) generally is first manifested above 850–900 °C.

The interpreted interval of $^{39}Ar$ release for each of the samples is listed in Table 2. Generally, the low-temperature limit ($f_{min}$) corresponds to the point in the age spectrum where indications of fluid-inclusion hosted low-temperature $^{40}Ar_E$ disappear (i.e., the $^{40}Ar/^{39}Ar$ ages begin to increase systematically). In the case of RG K-feldspar, evidence of $^{40}Ar_E$ continued to higher temperature. To improve our ability to interpret results from this sample, we performed isothermal duplicates up to 1100 °C and modeled only the ages yielded by the second, less affected steps (see Mahon et al., 1998, for additional details about this strategy). For most samples, we established the upper limit for analysis ($f_{max}$) at the fraction of $^{39}Ar$ release that corresponded to the final 1100 °C step. At higher temperatures evidence for melting in the form of dramatically elevated $^{39}Ar$ diffusivities is manifested. For samples with problematic high temperature behavior (i.e., intermediate age maxima or high-temperature $^{40}Ar_E$), we set $f_{max}$ to immediately below the point where these anomalies first became resolved.

Three-quarters of the 24 interpreted samples (AC, BM, BW2, CM1, CP128, CP175, CV, DSC, FCM, JU, LBV2B, MP, MP17, SFH, SP, SY, TS, and YS) yielded sufficiently well behaved age and Arrehnius properties that we felt confident in modeling all steps unaffected by low-temperature $^{40}Ar_E$ up to the point of melting (Table 2). K-feldspars from domain B had generally higher levels of low-temperature excess $^{40}Ar^{*}$. Unfortunately, we could not correct the age spectra of these samples for this effect since $^{38}Ar$ was not measured (see Harrison et al., 1994). In domain C, several K-feldspars (JU and MP) had relatively high age uncertainties that we attribute to small sample size due to the very K-feldspar–poor nature of the host rocks. Another sample (RG) had an inordinately large amount of low-temperature $^{40}Ar_E$. Additional samples in domains B, C, and D (CS, GM, KS, MMVT, and TG) exhibited intermediate maxima that significantly limited the interval of $^{39}Ar$ release ($f_{max}$ - $f_{min}$) that we were able to model (Table 2).

A subset of the samples discussed in this paper (AC, CP128, CP175, CV, FCM, JU, LBV2B, MP, MP17, SFH, SP, and SY) were previously analyzed in Grove (1993). Temperature cycling measurements (e.g., Lovera et al., 1989) that were performed with these samples are not presented here. While such experiments are very useful in elucidating the multi-diffusion character of $^{39}Ar$ release from K-feldspar, in practice it is difficult to adequately constrain temperature in the crucible during conditions of declining temperature. Specifically, sluggish thermal equilibration in the crucible (particularly at low temperature) causes more $^{39}Ar$ release than should have been the case if the sample temperature corresponded to the set temperature. Because diffusivities fall exponentially with temperature, the effect can be significant and lead to misleading results (i.e., dramatic and geologically unreasonable variation in activation energy is often implied; see Lovera et al., 1997). Because the fraction of $^{39}Ar$ release associated with these steps is generally very small (typically <0.1%), neglecting them has no discernible impact (relative to the ± 0.05 uncertainties in $D/r^2$) upon $^{39}Ar$ diffusivities of adjacent steps.

## APPENDIX 3 NUMERICAL SIMULATIONS

### Erosion Denudation

Our calculations of erosion denudation effects are modified after Lovera et al. (1999). We employed a two-dimensional, Crank-Nicholson finite-difference algorithm to solve the diffusion equation (Press et al.,

1986, p. 638). A constant thermal diffusivity ($10^{-6}$ m$^2$/s), no radioactive internal heating, and a fixed basal heat flux appropriate to maintain a 30 °C/km thermal gradient (= the initial geothermal gradient) were used. Calculations were performed in a 400-km-wide by 60-km-deep grid (1 km × 1 km resolution). Surface temperature was maintained constant at 25 °C and zero-flux conditions were established at the lateral boundaries. Calculations began at 125 Ma and terminated at 40 Ma. Random distributions of circular plutons with randomly specified radius and emplacement temperature were intruded at 2 m.y. intervals (see Lovera et al., 1999, for further details). Three distinct regions of intrusion were set up. For the region bounded by $120 < x < 175$ km (western Peninsular Ranges batholith), we intruded plutons at depths between 2 and 20 km from 120–100 Ma. For the region bounded by $175 < x < 230$ km (eastern Peninsular Ranges batholith), we intruded plutons at depths between 2 and 20 km from 105–90 Ma. Finally, for the region bounded by $230 < x < 400$ km (Salton Trough/Gulf of California and western Sonora), we intruded plutons at depths between 2 and 10 km from 90 to 65 Ma. Denudation was initiated at 108 Ma. In the model, progressively developed Late Cretaceous erosion surfaces were represented by propagating a 25 °C surface through the finite difference grid in successive time steps. This was accomplished by setting the temperature of all grid points situated at or above the defined surface to a constant value (25°C). The applied denudation history at $x = 215$ km shown in Figure 8C produced a final erosion depth of 20 km at 65 Ma. A proportionally scaled denudation history was applied at other lateral positions in the grid to produce the final erosion surface shown in Figure 8A. Temperature-time histories were recorded for each grid node in the model. Bulk closure ages were calculated assuming a single domain diffusion model and experimentally determined Arrhenius parameters for K-feldspar (activation energy or $E = 46$ kcal/mol; frequency factor or $\log D_o/r_o^2 = 3.5$ s$^{-1}$; Lovera et al., 1997). To calculate detrital age distributions, cooling ages were randomly sampled at 1 m.y. intervals between surfaces separated by ± 0.5 Ma. This procedure is described in more detail in Lovera et al. (1999).

### Subduction Refrigeration

We employed a two-dimensional, Crank-Nicholson finite-difference algorithm to solve the diffusion equation (Press, et al., 1986, p. 638). Heat conduction, boundary conditions, and the calculation grid dimensions and resolution were described in the same manner as for erosion denudation. In our calculations, shallow subduction was initiated at 80 Ma at $x = 75$ km. The slab dipped at 15° and was underthrust to the right at 4 cm/yr. We implemented a 2-km-thick shear zone characterized by a constant friction equivalent to 30 MPa. Temperature-time (T-t) histories were monitored continuously for all points within the 15 × 75 km region outlined in Figure 9A. K-feldspar closure ages were calculated as described above.

## ACKNOWLEDGMENTS

We acknowledge support from Department of Energy grant DE-FG-03-89ER14049. Grove received support from National Science Foundation grant EAR-0113563 as well as from additional NSF grants to Harrison. Vicki Todd was an invaluable source of information regarding local geology and contributed several key samples. Important information and insight regarding various aspects of the study have also come from discussions with Pat Abbott, Gary Axen, Brad Erskine, John Fletcher, Gordon Gastil, Peter George, Gary Girty, Laurel Goodwin, Dave Kimbrough, Cynthia Lampe, Harold Lang, Charlie Lough, Craig Manning, Doug Morton, Lothar Ratschbacher, Dave Rothstein, Keegan Schmidt, Lee Silver, Amy Stinson, Rich Wolf, and Mike Walawender. Dave Rothstein performed some of the $^{40}$Ar/$^{39}$Ar measurements included in this study. Matt Heizler was extremely helpful in supporting the $^{40}$Ar/$^{39}$Ar analysis and also helped in our initial attempts to interpret the results through the use of the MDD model. Reviews of this paper by Dave Kimbrough and Gary Girty helped to improve it considerably.

## REFERENCES CITED

Abbott, P.L., and Smith, T.E., 1978, Trace element comparison of clasts in Eocene conglomerates, southwestern California and northwestern Mexico: Journal of Geology, v. 86, p. 753–762.

Abbott, P.L., and Smith, T.E., 1989, Sonora, Mexico, source for the Eocene Poway Conglomerate of southern California: Geology, v. 17, p. 329–332.

Ague, J.J., Brandon, M.T., 1992, Tilt and northward offset of Cordilleran batholiths resolved using igneous barometry: Nature, v. 360, p. 146 152.

Ague, J.J., and Brimhall, G.H., 1988, Magmatic arc asymmetry and distribution of anomalous plutonic belts in the batholiths of California; effects of assimilation, crustal thickness, and depth of crystallization: Geological Society of America Bulletin, v. 100, p. 912–927.

Allmendinger, R.W., Figueroa, D., Snyder, D., Beer, J., Mpodozis, C., and Isacks, B.L., 1990, Foreland shortening and crustal balancing in the Andes at 30°S latitude: Tectonics, v. 9, p. 789–809.

Anderson, J.R., 1983, Petrology of a portion of the eastern Peninsular Ranges mylonite zone, Southern California: Contributions to Mineralogy and Petrology, v. 84, p. 253–271.

Anderson, T.H., and Silver, L.T., 1974, Late Cretaceous plutonism in Sonora, Mexico and its relationship to circum-Pacific magmatism: Geological Society of America Abstracts with programs, v. 6, no. 6, p. 484.

Armstrong, R.L., and Suppe, J., 1973, Potassium-argon geochronometry of Mesozoic igneous rocks in Nevada, Utah, and southern California: Geological Society of America Bulletin, v. 84, p. 1375–1392.

Axen, G.J., and Fletcher, J.M., 1998, Late Miocene—Pleistocene extensional faulting, northern Gulf of California, Mexico and Salton Trough, California: International Geology Review, v. 40, p. 217 244.

Axen, G.J., Grove, M., Stockli, D., Lovera, O.M., Rothstein, D.A., Fletcher, J.M., Farley, K., and Abbott, P.L., 2000, Thermal evolution of Monte Blanco Dome; low-angle normal faulting during Gulf of California rifting and late Eocene denudation of the eastern Peninsular Ranges: Tectonics, v. 19, p. 197–212.

Baird, A.K., and Miesch, A.T., 1984, Batholithic rocks of southern California—a model for the petrogenesis of their source materials: U.S. Geological Survey Professional Paper 1284, p. 42.

Bannon, J.L., Bottjer, D.J., Lund S.P., and Saul, L.R., 1989, Campanian/Maastrichtian stage boundary in southern California: Resolution and implications for large-scale depositional patterns: Geology, v. 17, p. 80–83.

Barth, A.P., Wooden, J.L., Grove, M., Jacobson, C.E., and Dawson, J.P., 2003, U-Pb zircon geochronology of rocks in the Salinas Valley region of California: A reevaluation of the crustal structure and origin of the Salinian Block: Geology, v. 31, p. 517–520.

Barton, M.D., Battles, D.A., Bebout, G.E., Capo, R.C., Christensen, J.N., Davis, S.R., Hanson, R.B., Michelsen, C.J., and Trim, H.E., 1988, Mesozoic contact metamorphism in the Western United States, in Ernst, W.G., ed., Metamorphism and crustal evolution of the Western United States, Rubey Volume VII: Englewood Cliffs, New Jersey, Prentice-Hall, p. 110–178.

Bateman, P.C., and Chappell, B.W., 1979, Crystallization, fractionation, and solidification of the Tuolumne Intrusive Series, Yosemite National Park, California: Geological Society of America Bulletin, v. 90, p. I 465-I 482.

Berggreen, R.G., and Walawender, M.J., 1977, Petrography and metamorphism of the Morena Reservoir roof pendant, southern California: California Division of Mines and Geology Special Report 129, p. 61–65.

Bird, P., 1988, Formation of the Rocky Mountains, western United States: A continuum computer model: Science, v. 239, p. 1501–1507.

Bottjer, D.J., and Link, M.H., 1984, A synthesis of Late Cretaceous southern California and northern Baja California paleogeography, *in* Crouch, J.K., and Bachman, S.B., eds., Tectonics and sedimentation along the California margin: Los Angeles, Society for Ecomonic Paleontologists and Mineralogists Pacific Section, p. 171–188.

Bottjer, D.J., Colburn, I.P., and Cooper, J.D., 1982, Late Cretaceous depositional environments and paleogeography, Santa Ana Mountains, Southern California: Los Angeles, Society for Ecomonic Paleontologists and Mineralogists Pacific Section, p. 121.

Burchfiel, B.C., and Davis, G.A., 1981, Mojave Desert and environs, *in* Ernst, W.G., ed., The geotectonic development of California, Rubey Vol. I: Englewood Cliffs, New Jersey, Prentice Hall, p. 217–252.

Butler, R.H., Dickinson, W.R., and Gerhels, G.E., 1991, Paleomagnetism of coastal California and Baja California: Alternatives to large-scale northward transport: Tectonics, v. 10, p. 561–576.

Cerveny, P.F., Dorsey, R.J., and Burns, B.A., 1991, Apatite and zircon fission-track ages from the Sierra San Pedro Martir, eastern Peninsular Range, Baja California, Mexico: Geological Society of America Abstracts with Programs, v. 23, no. 2, p. 12.

Chase, C.G., and Wallace, T.C., 1986, Uplift of the Sierra Nevada of California: Geology, v. 14, p. 730–733.

Clinkenbeard, J.P., and Walawender, M.J., 1989, Mineralogy of the La Posta pluton: Implications for the origin of zoned plutons in the eastern Peninsular Ranges batholith, southern and Baja California: American Mineralogist, v. 74, p. 1258–1269.

Coleman, D.S., and Glazner, A.F., 1998, The Sierra Crest magmatic event: Rapid formation of juvenile crust during the Late Cretaceous in California, *in* Ernst, W.G., and Nelson, C.A., eds., Integrated Earth and environmental evolution of the southwestern United States: Columbia, Maryland, Bellwether Publishing for the Geological Society of America, p. 253–272.

Coney, P.J., and Reynolds, S.J., 1977, Cordilleran Benioff zones: Nature, v. 270, p. 403–405.

Crowell, J.C., 1981, An outline of the tectonic history of southeastern California, *in* Ernst, W.G., ed., The geotectonic development of California (Rubey Vol. I): Englewood Cliffs, New Jersey, Prentice Hall, p. 583–600.

DePaolo, D.J., 1981, A neodymium and strontium isotopic study of the Mesozoic calc-alkaline granitic batholiths of the Sierra Nevada and Peninsular Ranges, California: Journal of Geophysical Research, v. 86, p. 10470–10488.

Detterman, M.E., 1984, Geology of the Metal Mountain district, In-ko-pah Mountains, San Diego County, California [M.S. thesis]: San Diego, San Diego State University, 216 p.

Dickinson, W.R., and Butler, R.F., 1998, Coastal and Baja California paleomagnetism reconsidered: Geological Society of America Bulletin, v. 110, p. 1268 1280.

Dickinson, W.R., and Snyder, W.S., 1978, Plate tectonics of the Laramide orogeny: Boulder, Colorado, Geological Society of America Memoir 151, p. 355–366.

Dodson, M.H., 1973, Closure temperature in cooling geochronological and petrological systems: Contributions to Mineralogy and Petrology, v. 40, p. 259–274.

Dokka, R.K., and Merriam, R.H., 1982, Late Cenozoic extension of northeastern Baja California, Mexico: Geological Society of America Bulletin, v. 93, p. 371–378.

Dorsey, R.J., 2002, Stratigraphic record of Pleistocene initiation and slip on the Coyote Creek fault, lower Coyote Creek, southern California, in Barth, A., ed., Contributions to crustal evolution of the southwestern United States: Boulder, Colorado, Geological Society of America Special Paper 365, p. 251 269.

Ducea, M., 2001, The California arc: Thick granitic batholiths, eclogite residues, lithospheric-scale thrusting, and magmatic flare-ups: GSA Today, v. 11, no. 11, p. 4–10.

Dumitru, T.A., 1990, Subnormal Cenozoic geothermal gradients in the extinct Sierra Nevada magmatic arc; consequences of Laramide and post-Laramide shallow-angle subduction: Journal of Geophysical Research, v. 95, p. 4925–4941.

Dumitru, T.A., Gans, P.B., Foster, D.A., and Miller, E.L., 1991, Refrigeration of the western Cordilleran lithosphere during Laramide shallow-angle subduction: Geology, v. 19, p. 1145–1148.

Engel, A.E.J., and Schultejann, P.A., 1984, Late Mesozoic and Cenozoic tectonic history of south central California: Tectonics, v. 3, no. 6, p. 659–675.

Erskine, B.G., and Wenk, H.R., 1985, Evidence for Late Cretaceous crustal thinning in the Santa Rosa mylonite zone, southern California: Geology, v. 18, p. 1173–1177.

Everden, J.F., and Kistler, R.W., 1970, Chronology of emplacement of Mesozoic batholithic complexes in California and western Nevada: U.S. Geological Survey Professional Paper 623, 42 p.

Everhart, D.L., 1951, Geology of the Cuyamaca Peak quadrangle, San Diego County, California: California Division of Mines Bulletin 159, p. 51–115.

Flynn, C.J., 1970, Post-batholithic geology of La Gloria Presa Rodriquez area, Baja California, Mexico: Geological Society of America Bulletin, v. 81, p. 1789–1806.

Fry, J.G., Bottjer, D.J., and Lund, S.P., 1985, Magnetostratigraphy of displaced Upper Cretaceous strata in southern California: Geology, v. 13, p. 648–651.

Gastil, R.G., 1979, A conceptual hypothesis for the relation of differing tectonic terranes to plutonic emplacement: Geology, v. 7, p. 542–544.

Gastil, R.G., 1983, Mesozoic and Cenozoic granitic rocks of southern California and western Mexico: Boulder, Colorado, Geological Society of America Memoir 159, p. 265–275.

Gastil, R.G., 1993, Prebatholithic history of peninsular California, *in* The prebatholithic stratigraphy of peninsular California: Geological Society of America Special Paper 279, p. 145–156.

Gastil, R.G., and Krummenacher, D., 1977, Reconnaissance geologic map of coastal Sonora between Puerto Lobos and Bahia Kino: Geological Society of America Bulletin, v. 88, p. 189–198.

Gastil, R.G., Phillips, R.P., and Allison, E.C., 1975, Reconnaissance geology of the state of Baja California: Boulder, Colorado, Geological Society of America Memoir 140, 170 p.

Gastil, R.G., Morgan, G.J., and Krummenacher, D., 1981, The tectonic history of peninsular California and adjacent Mexico, *in* Ernst, W.G., ed., The Geotectonic Development of California, Rubey Volume I: Englewood Cliffs, New Jersey, Prentice-Hall, p. 284–306.

Gastil, G., Diamond, J., Knaack, C., Walawender, M., Marshall, M., Boyles, C., and Chadwick, B., 1990, The problem of the magnetite/ilmenite boundary in southern and Baja California, *in* Anderson, J.L., ed., The nature and origin of Cordilleran magmatism: Boulder, Colorado, Geological Society of America Memoir 174, p. 19–32.

Gastil, G., Kimbrough, J., Tainosho, Y., Shimizu, M., and Gunn, S.H., 1991, Plutons of the eastern Peninsular Ranges, southern California, USA and Baja California, Mexico, in Walawender, M.J., and Hanan Hanan, B., Geological excursions in Southern California and Mexico: San Diego, San Diego State University Publication, p. 319 331.

George, P.G., and Dokka, R.K., 1994, Major Late Cretaceous cooling events in the eastern Peninsular Ranges, California, and their implications for Cordilleran tectonics: Geological Society of America Bulletin, v. 106, p. 903–914.

Germinario, M.P., 1993, The early Mesozoic Julian Schist, Julian, California: Boulder, Colorado, Geological Society of America Special Paper 279, p. 107–118, 1993.

Girty, G.H., 1987, Sandstone provenance, Point Loma formation, San Diego, California: Evidence for uplift of the Peninsular Ranges during the Laramide orogeny: Journal of Sedimentary Petrology, v. 57, p. 839–844.

Goodwin, L.B., and Renne, P.R., 1991, Effects of progressive mylonitization on Ar retention in biotites from the Santa Rosa mylonite zone, California, and thermochronologic implications: Contributions to Mineralogy and Petrology, v. 108, p. 283–297.

Gromet, L.P., and Silver, L.T., 1987, REE variations across the Peninsular Ranges batholith: Implications for batholithic petrogenesis and crustal growth in magmatic arcs: Journal of Petrology, v. 28, p. 75–125.

Grove, M., 1987, Metamorphism and deformation in the Box Canyon area, eastern Peninsular Ranges, San Diego County, California [M.S. thesis]: Los Angeles, University of California, 174 p.

Grove, M., 1993, Thermal histories of southern California basement terranes [PhD. thesis]: Los Angeles, University of California, 451 p.

Grove, M., 1994, Contrasting denudation histories within the east-central Peninsular Ranges batholith (33°N), *in* McGill, S.F., and Ross, T.M., Geological investigations of an active margin: Redlands, California, San Bernardino County Museum Association, p. 235–240.

Grove, M., Fletcher, J., Axen, G., and Stockli, D., 2003a, U-Pb zircon crystallization ages for plutonic rocks within the Sierra el Mayor and Sierra Cucapá, northwestern Baja California, México, Geological Society of America Abstracts with Programs, v. 35, no. 6, p. 27.

Grove, M., Jacobson, C.E., Barth, A.P., and Vucic, A., 2003b, Temporal and spatial trends of Late Cretaceous–early Tertiary underplanting of Pelona and related schist beneath southern California and southwestern Arizona, *in* Johnson, S.E., Paterson, S.R., Fletcher, J.M., Girty, G.H., Kimbrough, D.L., and Martín-Barajas, A., eds., Tectonic evolution of northwestern México and the southwestern USA: Boulder, Colorado, Geological Society of America Special Paper 374, p. 381–406 (this volume).

Grove, M., and Harrison, T.M., 1996, $^{40}Ar^{*}$ diffusion in Fe-rich biotite: American Mineralogist, v. 81, p. 940–951.

Hamilton, W., 1988, Tectonic setting and variations with depth of some Cretaceous and Cenozoic structural and magmatic systems of the western United States, *in* Ernst, W.G., ed., Metamorphism and crustal evolution of the western United States, Rubey Vol. VII: Englewood Cliffs, New Jersey, Prentice Hall, p. 1–40.

Hanson R.B., and Barton, M.D., 1989, Thermal development of low-pressure metamorphic belts: Results from two-dimensional numerical models: Journal of Geophysical Research, v. 94, p. 10363–10377.

Harrison, T.M., Heizler, M.T., Lovera, O.M., Chen, W., and Grove, M., 1994, A chlorine disinfectant for excess argon released from K-feldspar during step-heating: Earth and Planetary Science Letters, v. 123, p. 95–104.

Hill, R.I., 1988, San Jacinto intrusive complex 1. Geology and mineral chemistry, and a model for intermittent recharge of tonalitic magma chambers: Journal of Geophysical Research, v. 93, p. 10,325–10,348.

Hill, R.I., Silver, L.T., and Taylor, H.P., 1986, Coupled Sr-O isotope variations as an indicator of source heterogeneity for the northern Peninsular Ranges batholith: Contributions to Mineralogy and Petrology, v. 92, p. 351 361.

Hoggatt, W.C., 1979, Geologic map of Sweeney Pass Quadrangle, San Diego County, California: U.S. Geological Survey Open-File Report OF 79-754, 37 p.

Jachens, R.C., Simpson, R.W., Griscom, A., and Mariano, J., 1986, Plutonic belts in southern California defined by gravity and magnetic anomalies: Geological Society of America Abstracts with Programs, v. 18, p. 120.

Jennings, C.W., compiler, 1977, Geologic map of California: California Division of Mines and Geology, 1 sheet, scale: 1:750,000.

Kairouz, M., Axen, G.J., Grove, M., Lovera, O., and Stockli, D., 2003, Late Cenozoic $^{40}Ar/^{39}Ar$ ages of fault rocks formed along the west Salton detachment systems, southern California, Geological Society of America Abstracts with Programs, v. 35, no. 6, p. 629.

Kennedy, M.P., and Moore, G.W., 1971, Stratigraphic relations of Upper Cretaceous and Eocene formations, San Diego coastal area, California: American Association of Petroleum Geologists Bulletin, v. 55, p. 709–722.

Kies, R.P., and Abbott, P.L., 1983, Rhyolite clast populations and tectonics in the California continental borderland: Journal of Sedimentary Petrology, v. 53, p. 461–475.

Kimbrough, D.L., Magistrale, H., and Gastil, R.G., 1998, Enormous Late Cretaceous magma flux associated with TTG batholith emplacement; eastern Peninsular Ranges batholith of Southern and Baja California: Geological Society of America Abstracts with Programs, v. 30, no. 7, p. 258.

Kimbrough, D.L., Smith, D.P., Mahoney, J.B., Moore, T.E., Grove, M., Gastil, R.G., and Ortega-Rivera, A., 2001, Forearc-basin sedimentary response to rapid Late Cretaceous batholith emplacement in the Peninsular Ranges of southern and Baja California: Geology, v. 29, p. 491 494.

Kofron, R.J., 1984, Age and origin of gold mineralization in the southern portion of the Julian mining district, Southern California [M.S. thesis]: San Diego, San Diego State University, 75 p.

Krummenacher, D., Gastil, R.G., Bushee, J., and Doupont, J., 1975, K-Ar apparent ages, Peninsular Ranges batholith, southern California: Geological Society of America Bulletin, v. 86, p. 760–768.

Lampe, C.M., 1988, Geology of the Granite Mountain area; Implications of the extent and style of deformation along the southeast portion of the Elsinore fault [M.S. thesis]: San Diego, San Diego State University, 150 p.

Lewis, J.L., Day, S.M., Magistrale, H.C., Raul, R.A., Luciana, R., Cecilio, J., Eakins, J., Vernon, F.L., and Brune, J.N., 2001, Crustal thickness of the Peninsular Ranges and Gulf extensional province in the Californias: Journal of Geophysical Research, v. 106, p. 13,599–13,611.

Liou, J.G., Maruyama, S., and Cho, M., 1987, Very low-grade metamorphism of volcanic and volcaniclastic rocks—mineral assemblages and mineral facies, *in* Frey, M., ed., Low Temperature Metamorphism: Glasgow, Blackie, p. 59–113.

Lough, C.F., and Stinson, A.L., 1991, Structural evolution of the Vallecito Mountains, SW California: Geological Society of America Abstracts with Programs, v. 23, no. 5, p. 246.

Lovera, O.M., Richter, F.M., and Harrison, T.M., 1989, $^{40}Ar/^{39}Ar$ thermochronometry for slowly cooled samples having a distribution of diffusion domain sizes: Journal of Geophysical Research, v. 94, p. 17917–17935.

Lovera, O.M., Heizler, M.T., and Harrison, T.M., 1993, Argon diffusion domains in K-feldspar II: Kinetic properties of MH-10: Contributions to Mineralogy and Petrology, v. 113, p. 381–393.

Lovera, O.M., Grove, M., Harrison, T.M., and Mahon, K.I., 1997, Systematic analysis of K-feldspar $^{40}Ar/^{39}Ar$ step-heating experiments I: Significance of activation energy determinations: Geochimica et Cosmochimica Acta, v. 61, p. 3171–3192.

Lovera, O.M., Grove, M., Kimbrough, D.L., and Abbott, P.L., 1999, A method for evaluating basement exhumation histories from closure age distributions of detrital minerals: Journal of Geophysical Research, v. 104, p. 29,419–29,438.

Lovera, O.M., Grove, M., and Harrison, T.M., 2002, Systematic analysis of K-feldspar $^{40}Ar/^{39}Ar$ step-heating experiments II: Relevance of laboratory K-feldspar argon diffusion properties to nature: Geochimica Cosmochimica Acta, v. 66, p. 1237–1255.

Magistrale, H., and Rockwell, T.K., 1996, The central and southern Elsinore fault zone, southern California: Bulletin of the Seismological Society of America, v. 86, p. 1793–1803.

Mahon, K.I., Harrison, T.M., and Grove, M., 1998, The thermal and cementation histories of a sandstone petroleum reservoir, Elk Hills, California. 1: $^{40}Ar/^{39}Ar$ thermal history results, Chemical Geology, v. 152, p. 227–256.

Martin, H., 1993, The mechanics of petrogenesis of the Archean continental crust-comparison with modern processes: Lithos, v. 30, p. 373–388.

McDougall, I., and Harrison, T.M., 1999, Geochronology and thermochronology by the $^{40}Ar/^{39}Ar$ method: New York, Oxford University Press, 212 p.

McDowell, F.W., Roldán-Quintana, J., and Connelly, J.N., 2001, Duration of Late Cretaceous–early Tertiary magmatism in east-central Sonora, Mexico: Geological Society of America Bulletin, v. 113, p. 521–531.

Merriam, R.H., 1958, Geology of the Santa Ysabel quadrangle, San Diego County, California: California Division of Mines Bulletin, v. 177, p. 7–20.

Miller, W.J., 1935, A geologic cross section across the southern Peninsular Range of California: California Journal of Mines and Geology, v. 31, p. 115–242.

Miller, D.E., and Kato, T., 1991, Mid-Tertiary continental extension, SW Salton Trough, California: Geological Society of America Abstracts with Programs, v. 23, no. 2, p. 79.

Minch, J.A., 1979, The late-Mesozoic—Early Tertiary framework of continental sedimentation, northern Peninsular Ranges, Baja California, Mexico, *in* Abbott, P.L., ed., Eocene depositional systems: Los Angeles, Society for Sedimentary Geology Pacific Section, p. 43–68.

Murray, G.T., and Girty, G.H., 1996, Pre-Jurassic deformation and metamorphism within the Julian Schist, Peninsular Ranges, Southern California: Geological Society of America Abstracts with Programs, v. 28, no. 5, p. 95.

Naeser, C.W., Naeser, N.D., Todd, V.R., Bohannon, R.G., 1996, Thermochrononology of the Peninsular Ranges Batholith, Southern California, from fission-track and $^{40}Ar/^{39}Ar$ analysis, Geological Society of America Abstracts with Programs, v. 28, no. 7, p. 513.

Nilsen, T.H., and Abbott, P.L., 1981, Paleogeography and sedimentology of Upper Cretaceous turbidites, San Diego, California: American Association of Petroleum Geologists Bulletin, v. 65, p. 1256–1284.

Nordstrom, C.E., 1970, Lusardi Formation—A post-batholithic Cretaceous conglomerate north of San Diego, California: Geological Society of America Bulletin, v. 81, p. 601–605.

Ortega-Gutierrez, F., Mitre-Salazar, L.M., Roldán-Quintana, J., Aranda-Gómez, J., Morán-Zenteno, D.J., Alanís-Alvarez, S., and Nieto-Samaniego, A., 1992, Carta geológica de la República Mexicana, escala 1:2,000,000, quinta edición: Secretaria de Minas e Industria Par-aestatal, Consejo de Recursos Minerales y Universidad Nacional Autónoma de México, Instituto de Geología.

Ortega-Rivera, A., 2003, Geochronological constraints on the tectonic history of the Peninsular Ranges batholith of Alta and Baja California: Tectonic Implications for western México, *in* Johnson, S.E., Paterson, S.R., Fletcher, J.M., Girty, G.H., Kimbrough, D.L., and Martín-Barajas, A., eds., Tectonic evolution of northwestern México and the southwestern USA: Boulder, Colorado, Geological Society of America Special Paper 374, p. 297–335 (this volume).

Ortega-Rivera, A., Farrar, E., Hanes, J.A., Archibald, D.A., Gastil, R.G., Kimbrough, D.L., Zentilli, M., Lopez, M.M., Feraud, G., and Ruffet, G., 1997, Chronological constraints on the thermal and tilting history of the Sierra San Pedro Martir Pluton, Baja California, Mexico, from U/Pb, $^{40}Ar/^{39}Ar$, and fission-track geochronology: Geological Society of America Bulletin, v. 109, p. 728 745.

Parrish, K.E., 1990, Geology, petrology, geochemistry, and isotopic character of the Indian Hill pluton, Jacumba Mountains [M.S. thesis]: San Diego, San Diego State University, 136 p.

Parsons, I., Brown, W.L., and Smith J.V., 1999, $^{40}Ar/^{39}Ar$ thermochronology using alkali feldspars: Real thermal history or mathematical mirage of microtexture?: Contributions to Mineralogy and Petrology, v. 136, p. 92–110.

Peterson, G.L., and Nordstrom, C.E., 1970, Sub-La Jolla unconformity in vicinity of San Diego, California: American Association of Petroleum Geologists Bulletin, v. 54, p. 265–274.

Phillips, E., 1964, Coaxial refolding in southeast San Diego County, California [M.S. thesis], San Diego, San Diego State College, 30 p.

Premo, W., Morton, D.M., Snee, L., Naeser, N.D., and Fanning, C.M., 1998, Isotopic ages, cooling histories, and magmatic origins for Mesozoic tonalitic plutons from the N. Peninsular Ranges batholith, S. California: Geological Society of America Abstracts with Programs, v. 30, no. 5, p. 59–60.

Press, W.H., Flannery, B.P., Teukolsky, S.A., and Vetterling, W.T., 1986, Numerical recipes: The art of scientific computing: Cambridge University Press, New York, 818 p.

Quidelleur, X., Grove, M., Harrison, T.M., and Yin, A., 1997, Thermal evolution and slip history of the Renbu Zedong thrust, southeastern Tibet: Journal of Geophysical Research, v. 102, p. 2659–2679.

Rothstein, D.A., and Manning, C.E., 2003. Geothermal gradients in continental magmatic arcs: Constraints from the eastern Peninsular Ranges batholith, Baja California, México, *in* Johnson, S.E., Paterson, S.R., Fletcher, J.M., Girty, G.H., Kimbrough, D.L., and Martín-Barajas, A., eds., Tectonic evolution of northwestern México and the southwestern USA: Boulder, Colorado, Geological Society of America Special Paper 374, p. 337–354 (this volume).

Schultejann, P.A., 1984, The Yaqui Ridge antiform and detachment fault: Mid-Cenozoic extensional terrane west of the San Andreas fault: Tectonics, v. 3, no. 6, p. 677–691.

Sharp, R.V., 1967, San Jacinto fault zone in the Peninsular Ranges of Southern California: Geological Society of America Bulletin, v. 78, p. 705 729.

Sharp, R.V., 1979, Some characteristics of the eastern Peninsular Ranges mylonite zone, *in* Proceedings, Conference VIII, Analysis of actual fault zones in bedrock: U.S. Geological Survey Open File Report 79-1239, p. 258–267.

Shaw, S.E., Todd, V.R., and Grove, M., 2003, Jurassic peraluminous gneissic granites in the axial zone of the Peninsular Ranges, southern California, *in* Johnson, S.E., Paterson, S.R., Fletcher, J.M., Girty, G.H., Kimbrough, D.L., and Martín-Barajas, A., eds., Tectonic evolution of northwestern México and the southwestern USA: Boulder, Colorado, Geological Society of America Special Paper 374, p. 157–183(this volume).

Siem, M.E., and Gastil, R.G., 1994, Mid-Tertiary to Holocene extension associated with the development of the Sierra El Mayor metamorphic core complex, northeastern Baja California, Mexico, *in* McGill, S.F., and Ross, T.M., Geological investigations of an active margin, GSA Cordilleran Section Guidebook: Redlands, California, San Bernardino County Museum Association, p. 107–119.

Silver, L.T., and Chappell, B., 1988, The Peninsular Ranges batholith: An insight into the evolution of the Cordilleran batholiths of southwestern North America: Transactions of the Royal Society of Edinburgh: Earth Sciences, v. 79, p. 105–121.

Silver, L. T, Taylor, H.P., Jr., and Chappell, B., 1979, Some petrological, geochemical and geochronological observations of the Peninsular Ranges batholith near the International Border of the U.S.A., and Mexico, *in* Abbott, P.L., and Todd, V.R., eds., Mesozoic Crystalline Rocks—Peninsular Ranges Batholith and Pegmatites, Point Sal Ophiolite: Geological Society of America Annual Meeting Guidebook: San Diego, San Diego State University, p. 83–110.

Silver, L.T., Chappell, B.C., and Anderson, T.H., 1996, Petrogenetic implications of petrographic and geochemical zonations in the integrated Peninsular Ranges and Sonoran batholiths: Geological Society of America Abstracts with Programs, v. 28, no. 5, p. 112.

Simpson, C., 1984, Borrego Springs–Santa Rosa mylonite zone—A Late Cretaceous west-directed thrust in southern California: Geology, v. 12, p. 8–11.

Staude, J.M.G., and Barton, M.D., 2001, Jurassic to Holocene tectonics, magmatism, and metallogeny of northwestern Mexico: Geological Society of America Bulletin, v. 113, p. 1357–1374.

Steiger, R.H., and Jäger, E., 1977, Subcommission on geochronology: Convention on the use of decay constants in geo- and cosmochronology: Earth and Planetary Science Letters, v. 36, p. 359–362.

Strand, R.G., 1962, Geologic map of California, San Diego–El Centro sheet, Olaf P. Jenkins edition: Sacremento, California Division of Mines and Geology, scale 1:250,000.

Sundberg, F.A., and Cooper, J.D., 1978, Late Cretaceous depositional environments, northern Santa Ana Mountains, Southern California, *in* Howell, D.G., and McDougall, K.A., eds., Mesozoic paleogeography of the western United States: Pacific Coast Paleogeography Symposium 2,: Los Angeles, Society of Economic Paleontologists and Mineralogists Pacific Section, , p. 535–546.

Taylor, H.P., 1986, Igneous rocks; 2, Isotopic case studies of Circum-Pacific magmatism, *in* Valley, J.W., Taylor, H.P., Jr., and O'Neil, J.R., eds., Stable isotopes in high-temperature geological processes: Reviews in Mineralogy, v. 16 p. 273–317.

Theodore, T.G., 1970, Petrogenesis of mylonites of high metamorphic grade in the Peninsular Ranges of southern California: Geological Society of America Bulletin, v. 81, p. 435–450.

Thomson, C.N., and Girty, G.H., 1994, Early Cretaceous intra-arc ductile strain in Triassic-Jurassic and Cretaceous continental margin arc rocks, Peninsular Ranges, California: Tectonics, v. 13, p. 1108 1119.

Tobisch, O.T., Saleeby, J., Renne, P.R., McNulty, B.A., and Tong, W., 1995, Variations in deformation fields during emplacement of a large-volume magmatic arc, central Sierra Nevada, California: Geological Society of America Bulletin, v. 107, p. 148–166.

Todd, V.R., 1977a, Geologic map of the Agua Caliente Springs Quadrangle, San Diego County, California: U.S. Geological Survey Open-File Report OF 77-0742, 20 p.

Todd, V.R., 1977b, Geologic map of the Cuyamaca Peak quadrangle, San Diego County, California: U.S. Geological Survey Open File Report 77-405, 13 p.

Todd, V.R., 1978, Geologic map of the Monument Peak quadrangle, San Diego County, California: U.S. Geological Survey Open File Report 78-697, 47 p.

Todd, V.R., 1979, Geologic map of the Mount Laguna quadrangle, San Diego County, California: U.S. Geological Survey Open File Report 79-862, 49 p.

Todd, V.R., and Shaw, S.E., 1979, Structural, metamorphic and intrusive framework of the Peninsular Ranges batholith in southern San Diego County, California, *in* Abbott, P.L., and Todd, V.R., eds., Mesozoic crystalline rocks—Peninsular Ranges batholith and pegmatites, Point Sal Ophiolite, Geological Society of America Annual Meeting Guidebook: San Diego, San Diego State University, p. 177–231.

Todd, V.R., and Shaw, S.E., 1985, S-type granitoids and an I-S line in the Peninsular Ranges batholith, southern California: Geology, v. 13, p. 231–233.

Todd, V.R., Shaw, S.E., and Hammarstrom, J.M., 2003, Cretaceous plutons of the Peninsular Ranges batholith, San Diego and westernmost Imperial Counties, California: Intrusion across a Late Jurassic continental margin, *in* Johnson, S.E., Paterson, S.R., Fletcher, J.M., Girty, G.H., Kimbrough, D.L., and Martín-Barajas, A., eds., Tectonic evolution of northwestern México and the southwestern USA: Boulder, Colorado, Geological Society of America Special Paper 374, p. 185–235 (this volume).

Todd, V.R., Erskine, B.G., and Morton, D.M., 1988, Metamorphic and tectonic evolution of the northern Peninsular Ranges batholith, southern California, *in* Ernst, W.G., ed., Metamorphism and Crustal Evolution of the Western United States, Rubey Volume VII: Englewood Cliffs, New Jersey, Prentice-Hall, p. 894–937.

Walawender, M.J., Gastil, R.G., Clinkenbeard, J.P., McCormick, W.V., Eastman, B.G., Wernicke, R.S., Wardlaw, M.S., Gunn, S.H., and Smith, B.M., 1990, Origin and evolution of the zoned La Posta-type plutons, eastern Peninsular Ranges batholith, southern and Baja California, *in* Anderson, J.L., ed., The nature and origin of Cordilleran magmatism: Geological Society of America Memoir 174, p. 1–18.

Walawender, M.J., Girty, G.H., Lombardi, M.R., Kimbrough, D., Girty, M.S., and Anderson, C., 1991, A synthesis of recent work in the Peninsular Ranges batholith: Geological Society of America Annual Meeting Guidebook for Field Trips, p. 297–312.

Wenk, H.-R., Johnson, L.R., and Ratschbacher, L., 2000, Pseudotachylites in the eastern Peninsular Ranges of California: Tectonophysics, v. 321, p. 253 277.

Wolf, R.A., Farley, K.A., and Silver, L.T., 1997, Assessment of (U-Th)/He thermochronometry; the low-temperature history of the San Jacinto Mountains, California: Geology, v. 25, p. 65 68.

Manuscript Accepted by the Society June 2, 2003

Printed in the USA